JOURNAL OF GEOPHYSICAL RESEARCH, VOL. 113, D04212, doi:10.1029/2007JD009029, 2008

Aerosol direct radiative effects over Kanpur in the Indo-Gangetic basin, northern India: Long-term (2001–2005) observations and implications to regional climate

Sagnik Dey[1] and S. N. Tripathi[1]

Received 31 May 2007; revised 24 October 2007; accepted 28 November 2007; published 29 February 2008.

[1] We present 5-year (2001–2005) monthly mean estimates of direct radiative effects (DRE) due to aerosols over Kanpur region in the Indo-Gangetic basin for the first time. Further, the monthly and annual heterogeneity of aerosol DRE has been evaluated on the basis of the anthropogenic and natural aerosol contribution. An optically equivalent model has been formulated on the basis of the surface measurements, altitude profiles of aerosol properties in conjunction with remotely retrieved aerosol parameters, and the optical properties are used to estimate the aerosol DRE at the top-of-atmosphere (TOA), surface and atmosphere in the shortwave (SW) and longwave (LW) region. Water-solubles, black carbon (BC), and dust in fine ($dust_f$) and coarse ($dust_c$) mode are considered to be the main aerosol components on the basis of the chemical composition measurements. Anthropogenic components (scattering water-solubles and absorbing BC) contribute more than 80% to the composite aerosol optical depth, AOD (at 0.5 μm) in the winter, whereas the natural dusts contribute more than 55% in the summer months. Aerosols induce large negative surface forcing (more than -20 W m^{-2}) with higher values (more than -30 W m^{-2}) during the premonsoon season, when the transported natural dusts add to the anthropogenic aerosol pollution. The SW surface cooling is partially (maximum up to 11%) compensated by LW surface heating. The SW cloudy-sky aerosol DRE values are $+1.4 \pm 6.1$, -23.3 ± 9.3 and $+24.8 \pm 9.7$ W m^{-2} for TOA, surface and atmosphere, respectively. Annually $\sim$5% BC mass fraction contributes $\sim$9% to total $AOD_{0.5}$, but $\sim$40% to the total aerosol surface DRE. The annual mean (±SD) TOA, surface and atmospheric clear-sky SW anthropogenic aerosol DRE over Kanpur are $+0.3 \pm 2.5$, -19.9 ± 9 and $+20.2 \pm 9.9$ W m^{-2}, respectively. Large negative surface forcing and positive atmospheric forcing in the Kanpur region raise several climatic issues. Anthropogenic aerosols contribute 65.4% to the mean (±SD) annual heating rate of 0.84 ± 0.3 K d^{-1} over Kanpur. A persistently large reduction of net surface radiation would affect the regional hydrological cycle through changes in evaporation and sensible heat flux. Our study assesses the aerosol direct radiative effects in Kanpur region for a 5 year period, which would provide a baseline to more thoroughly address these climate-related issues in the future.

Citation: Dey, S., and S. N. Tripathi (2008), Aerosol direct radiative effects over Kanpur in the Indo-Gangetic basin, northern India: Long-term (2001–2005) observations and implications to regional climate, *J. Geophys. Res.*, *113*, D04212, doi:10.1029/2007JD009029.

1. Introduction

[2] Aerosols exert direct radiative effects (DRE) through scattering and absorption of sunlight [*Houghton et al.*, 2001; *Satheesh and Ramanathan*, 2000], but the magnitude and variability of the effect depends on the relative proportion of the anthropogenic and natural components, as they have distinct characteristics and size distributions [*Houghton et al.* 2001; *Kaufman et al.*, 2002, 2005; *Chung et al.*, 2005]. The DRE due to aerosols is defined as the effect of aerosols (both natural and anthropogenic) on the radiative fluxes. Similarly, the change in radiative flux due to only anthropogenic aerosols can be termed as aerosol direct radiative forcing (DRF) [*Chung et al.*, 2005]. Aerosols also modify the Earth's radiation budget through interaction with clouds (indirect effect) and hence affect the hydrological cycle [*Ramanathan et al.*, 2001a]. In regions, where both anthropogenic and natural aerosols play important roles in modifying the climate, proper assessment of anthropogenic aerosol forcing is also required to understand its role in long-term climate change.

[1]Department of Civil Engineering, Indian Institute of Technology, Kanpur, India.

0148-0227/08/2007JD009029$09.00

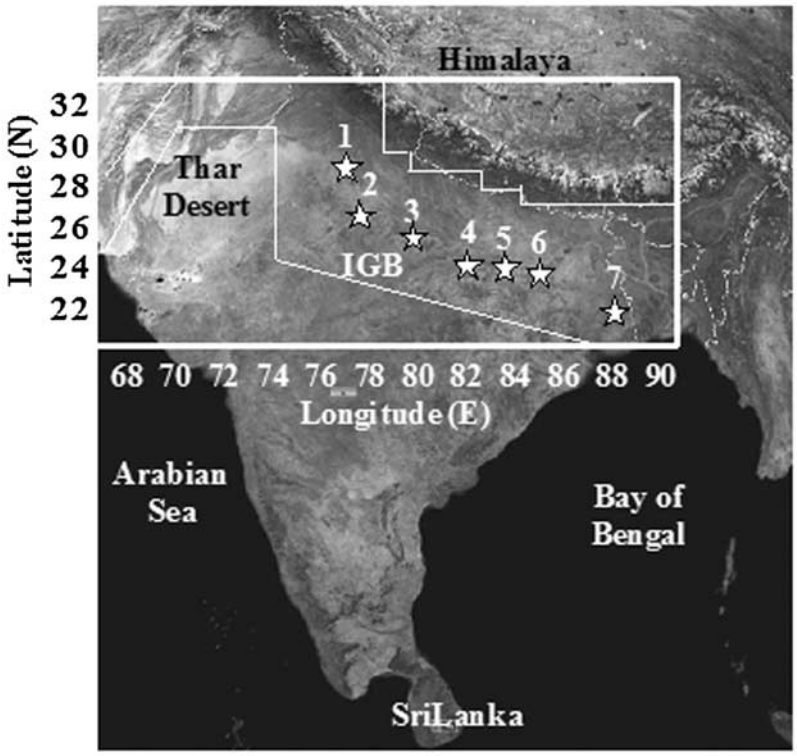

Figure 1. Indo-Gangetic Basin (IGB, demarcated by box within the physical map of Indian subcontinent) surrounded by the Himalayan mountain range, Thar Desert and the oceans. The major cities lying in the central part of IGB are marked by stars, numbers 1, 2, 3, 4, 5, 6 and 7 representing Delhi, Agra, Kanpur, Allahabad, Varanasi, Patna and Kolkata.

[3] The Indo-Gangetic basin (IGB) in India (Figure 1) is such a region, where anthropogenic and natural aerosols show distinct seasonal characteristics and mixing [*Dey et al.*, 2004, 2005; *Singh et al.*, 2004, 2005; *Chinnam et al.*, 2006; *Tripathi et al.*, 2005a, 2005b, 2006; *Tare et al.*, 2006]. The low-lying IGB is bordered by the Himalayan mountain range in the north, Thar Desert and Arabian Sea in the west, Bay of Bengal in the east and central Indian peninsula in the south. It stretches from Pakistan in the west (68°E longitude) to Bangladesh in the east (91°E longitude) encompassing most of the northern India (within 22 to 32°N latitude range). IGB houses more than 600 million people and is the most populated river basin in the world. Topographically, IGB is homogeneous with fluvial landforms and fertile lands rich in agricultural production. Increasing burden of population in the IGB has led to rapid urbanization and change in the land use pattern. The IGB as compared to other regions in India experiences four distinct seasons, winter (December–February), premonsoon (March–May), monsoon (June–September) and postmonsoon (October–November).

[4] In terms of aerosol loading, IGB is one of the most polluted regions in the world [*Girolamo et al.*, 2004; *Ramanathan and Ramana*, 2005; *Jethva et al.*, 2005; *Tripathi et al.*, 2006; *Ganguly et al.*, 2006; *Dey and Tripathi*, 2007]. The industrial growth, increasing usage of fossil fuel and other sources lead to massive aerosol load in the region [*Ramanathan and Ramana*, 2005; *Tripathi et al.*, 2006; *Dey and Tripathi*, 2007]. The greenhouse gases and the atmospheric brown clouds emitted by anthropogenic activities in the region reduce the agricultural crop production due to adverse changes in the regional climate [*Auffhammer et al.*, 2006]. Besides the anthropogenic pollution, natural aerosols (mostly dust) contribute to the regional aerosol loading in the summer months [*Dey et al.*, 2004; *Chinnam et al.*, 2006], altering the aerosol optical properties and radiative effects. Although there are numerous studies on the estimations of the aerosol DRE outside the Indian subcontinent [see *Bates et al.*, 2006; *Yu et al.*, 2006, and references therein], a limited number of studies have been done in the Indian subcontinent and even fewer in the IGB. No previous study in India has included 5 year continuous data sets to study long-term trends in the aerosol DRE; all of them were for much shorter duration. Aerosol DRE estimates in the IGB exists only for Delhi [*Ganguly et al.*, 2006], Hissar [*Ramachandran et al.*, 2006] and Nainital [*Pant et al.*, 2006], that too for one month. *Ramanathan and Ramana* [2005] have calculated aerosol DRE over the IGB using data collected over Kathmandu, Nepal for a 3 year period, but this site is located in the foothills of the Himalayas, north of the IGB.

[5] Kanpur (26.47°N latitude, 80.33°E longitude, 142 m above mean sea level), an urban/industrial site, is located in the central part of the IGB and earlier studies have confirmed the huge aerosol load over this region [*Singh et al.*, 2004; *Dey et al.*, 2004, 2005, 2006; *Dey and Tripathi*, 2007; *Chinnam et al.*, 2006; *Tripathi et al.*, 2005a, 2005b, 2006; *Tare et al.*, 2006]. The high aerosol loading not only

influences the cloud microphysical properties over Kanpur, but over the entire IGB [*Tripathi et al.*, 2007a]. Previous studies have assessed the seasonal variability of the aerosols in this region, the influence of the dust events on the aerosol optical properties and estimated the aerosol DRE for only few months duration. However, none of them addressed how seasonal variations in aerosol optical properties affect the regional climate, how clouds might affect the aerosol DRE in this region, and how much the contribution of anthropogenic fraction to the composite aerosol DRE could be.

[6] In this paper, we report, for the first time, monthly mean 5-year (2001–2005) estimations of DRE due to aerosols over Kanpur using ground-based and satellite observations and through a regional aerosol optical model. In the next section, the formulation of the optically equivalent aerosol model is discussed. The results are described in three parts; first, we describe composite aerosol DRE, then the anthropogenic aerosol DRF and finally their implications on the regional climate are discussed.

2. Methodology and Data Analysis

[7] The integration of surface observations and satellite data in assessing aerosol DRE was successfully implemented during Indian Ocean Experiment, INDOEX [*Ramanathan et al.*, 2001b; *Satheesh et al.*, 1999, 2002]. We have adopted a similar approach here for estimation of composite aerosol DRE, but adopted a different approach for anthropogenic aerosol DRF. The calculations are done for the 5 year period of 2001–2005.

2.1. Formulation of Aerosol Optical Model

[8] For this study, we have developed an optically equivalent aerosol model, considering the major anthropogenic (water-solubles, wsol, and black carbon, BC) and natural (dust) components [*Tare et al.*, 2006] in this region, which can simulate the optical properties comparable to the direct observations within the instruments' retrieval and measurements' uncertainty. Water solubles are the particles originating from gas-to-particle conversion and consist of sulfates, nitrates etc. [*Hess et al.*, 1998]. *Tare et al.* [2006] have presented a detailed chemical analysis of the aerosols in Kanpur region during a campaign and categorized the sources into soil-derived, gas-to-particle conversion and biomass burning. The unanalyzed part consists of carbonaceous aerosols, of which BC was measured by Aethalometer. The size distribution of the major cations and anions revealed that they are produced by anthropogenic activities [*Tare et al.*, 2006]. Even the biomass burning in this region is anthropogenic, not natural. The only limitation is that we do not have any data on organics and hence included them in water-solubles. There may be uplifting of dusts due to man-made erosion activities, but earlier studies have mentioned that the major source of dusts in this region is natural [*Singh et al.*, 2004; *Dey et al.*, 2004; *Chinnam et al.*, 2006]. Ground-based aerosol measurements have been carried out in Kanpur by Aerosol Robotic Network (AERONET) Sun photometer [*Singh et al.*, 2004] since 2001, which include spectral aerosol optical depth (AOD), single scattering albedo (SSA), asymmetry parameter (g), volume size distribution and refractive indices (both real and imaginary). Spectral AOD is derived at 7 wavelengths (0.34, 0.38, 0.44, 0.5, 0.67, 0.87 and 1.02 μm) in the visible to infrared wavelength region, whereas the other optical properties are retrieved at 4 wavelengths (0.44, 0.67, 0.87, 1.02 μm) [*Holben et al.*, 1998; *Dubovik and King*, 2000]. Retrieved optical properties from AERONET represent composite aerosols, hence it is important to differentiate the anthropogenic components from the natural aerosols to assess the anthropogenic contribution to the total aerosol DRE. Moreover, AERONET provides optical properties in the UV to NIR range (0.34 to 1.02 μm) and the extrapolation of the optical properties in the entire SW and LW region would induce errors in the estimation of the aerosol DRE. Hence the AERONET data are used to constrain the model results through which the role of the individual component to the composite aerosol is assessed.

[9] Among the four components, BC number concentration is calculated from the measured data for the entire period using the BC size distribution parameters of OPAC (Optical Properties of Aerosols and Clouds) data set [*Hess et al.*, 1998]. Surface equivalent BC concentration was measured by an Aethalometer (model AE-21-ER, Magee Scientific, USA) from December 2004 to December 2005. For the earlier period (January 2001 to November 2004), we have considered the columnar BC inferred from the AERONET measurements [*Dey et al.*, 2006]. The overall uncertainty in retrieval of columnar BC from AERONET retrievals is $\sim$10%, which is quite similar to the uncertainty of equivalent BC mass concentration measured by Aethalometer [*Babu and Moorthy*, 2002]. Once the number concentration of BC is fixed, the number concentrations of the other components are varied in the OPAC model iteratively, so that the model-derived optical properties match with the AERONET-retrieved optical properties under certain model constraints. The aerosol data set in OPAC are modeled to represent aerosols of particular type or origin [*Hess et al.*, 1998]. *Satheesh and Srinivasan* [2006] have shown that optically equivalent models developed using OPAC size distributions and constrained by direct measurements of composite aerosol properties can be used to estimate aerosol DRE accurately, if the size-segregated chemical compositions of various components are unavailable. However, the uncertainty in the aerosol DRE can be reduced if such measurements are available. For winter season, we have used the mass size distribution parameters of various individual species measured during a land campaign in Kanpur [*Dey and Tripathi*, 2007]. Hence, for the winter season, the calculated number size distribution parameters from *Dey and Tripathi* [2007] are used to simulate the aerosol optical properties. The number size distribution parameters derived from in situ measurements differ at most by 15% from the OPAC size distribution parameters [*Hess et al.*, 1998]. For other seasons, because of absence of size-separated chemical composition data, the default size distribution parameters from OPAC database are used. The extinction coefficient (b^{ext}), scattering coefficient (b^{sca}), absorption coefficient (b^{abs}), SSA, g and AOD at 61 wavelengths (between 0.25 and 40 μm) are simulated for 8 relative humidity values (RH of 0, 50, 70, 80, 90, 95, 98 and 99%). The RH was being measured by an automatic weather station deployed at IIT-K campus from December 2004 onward. The instrument measures the ambient RH at

Table 1. List of Measured or Retrieved Parameters Used in the Formulation of the Optically Equivalent Aerosol Model for Kanpur Region

Parameters	Instruments	Type	Period
BC concentration	aethalometer	in situ surface measurements	Dec 2004 onward
BC concentration	AERONET	retrieval using *Dey et al.* [2006] algorithm	Jan 2001 to Nov 2004
Aerosol altitude profile	optical particle counter	aircraft measurements (up to 2 km)	Jun 2006 and Oct 2006
BC altitude profile	aethalometer	aircraft measurements (up to 2 km)	Jan 2005, Jun 2006 and Oct 2006
AOD_λ	AERONET	ground-based retrieval	Jan 2001 to Dec 2005
SSA_λ	AERONET	ground-based retrieval	Jan 2001 to Dec 2005
g_λ	AERONET	ground-based retrieval	Jan 2001 to Dec 2005
Size-separated chemical composition	high volume sampler and Anderson impactor	sampling and chemical analysis [*Tare et al.*, 2006]	Dec 2004 to Jan 2005
Meteorological parameters	automatic weather station	direct in situ measurements	Dec 2004 onward

each 5 min interval each day. We have averaged the daytime measurements to obtain the monthly averaged RH for each month at Kanpur region. The optical properties of the composite aerosol at the RH closest to the monthly mean ambient RH are considered for the comparison.

[10] As we do not have real-time vertical profile of aerosol extinction, we assume that the distribution of aerosols in vertical column would be similar to the BC altitude profile derived from aircraft measurements during January 2005 [*Tripathi et al.*, 2005b] for the winter season, which shows that most of the particles are present within the boundary layer. Aerosol vertical profile over Delhi during December 2004 from Lidar measurements [*Ganguly et al.*, 2006] has also proved that most of the aerosols are confined within 1 km, above which the aerosol extinction becomes low and constant, during the winter season. From the measurement, the scale height for the winter season is calculated to be ~1.2 km. For the premonsoon and postmonsoon seasons, the respective BC and total aerosol concentration profiles [*Tripathi et al.*, 2007b] are measured using an aircraft. The measured BC and aerosol concentrations at different altitudes along the altitude profile are fitted in OPAC model to estimate the BC and total aerosol number concentration at the corresponding heights constrained by the observed BC mass fraction (f_{BC}). From the aerosol number concentration at different altitudes, the scale height of the aerosols is calculated to be ~1.3 km for these seasons. As there is no information available for the aerosol scale height for the monsoon season, the value for the premonsoon and postmonsoon seasons is assumed. The instruments and duration of measurements of various parameters used in formulation of the optical model are summarized in Table 1.

2.2. Model Constraints

[11] The optically equivalent aerosol model is constrained with following conditions: (1) $\chi^2 = \left(\frac{1}{n}\left(\sum_{\lambda=1}^{n}\left(AOD_{\lambda,AERONET} - AOD_{\lambda,Model}\right)^{1/2}\right)\right)$ should be less than 0.025, which is comparable to the retrieval error of observed AOD. (2) Angstrom exponent (α) of the model and AERONET retrieval should match within ±5%, so that the overestimation at the shorter wavelength and underestimation at the higher wavelength or vice versa should not lead to attaining minimum χ^2 [*Satheesh and Srinivasan*, 2006] for AOD spectrum. (3) Model-derived SSA_λ and g_λ should lie within ±5% of AERONET-retrieved SSA and g at all four wavelengths, as the accuracy of AERONET retrieval is 5% [*Dubovik et al.*, 2000].

[12] During the iteration, first the number concentration of water-solubles is set to the default value of "continental polluted" model of OPAC. The number concentrations of dust in fine and coarse mode are set to zero. Only the BC number concentration is set to be fixed during iteration. The number concentrations are then increased until the above said all three criteria are satisfied. For comparison of the model-derived composite aerosol optical properties with AERONET retrievals, we chose 7 wavelengths (0.35, 0.4, 0.45, 0.5, 0.65, 0.9 and 1 μm) for AOD_λ and four wavelengths (0.45, 0.65, 0.9 and 1.025 μm) for SSA_λ and g_λ, which are closest to the AERONET retrieval channels. As the model calculates the optical properties at various RH, to make proper comparison, the individual optical properties at RH closest to the ambient RH are selected. Then the composite SSA_λ and g_λ are calculated using the following relations:

$$SSA_\lambda = \frac{\sum_i b_{i,\lambda}^{ext} SSA_{i,\lambda}}{\sum_i b_{i,\lambda}^{ext}} \text{ and } g_\lambda = \frac{\sum_i b_{i,\lambda}^{sca} g_{i,\lambda}}{\sum_i b_{i,\lambda}^{sca}}, \quad (1)$$

where the subscript "i" denotes the corresponding optical property for a single component, b^{ext} and b^{sca} are the extinction and scattering coefficients of the individual component at a given wavelength λ. Composite AOD_λ is calculated by summing up the individual AOD_λ. Equation (1) simply represents the weighted average of the optical property of all the components.

[13] Another factor to be considered here is the spectral match of the optical properties. The AERONET provides the optical properties at slightly different wavelengths as compared to the model outputs. As the optical properties vary spectrally, to have desired match, the wavelengths should be similar. Hence the AERONET-retrieved optical properties are interpolated to the wavelengths at which the model-derived optical properties are calculated. We have followed the nonlinear interpolation technique as suggested by *Tripathi et al.* [2005c], which uses a second-order polynomial equation for interpolation.

[14] For the anthropogenic aerosol DRF, the anthropogenic aerosol optical properties are simulated considering the optical properties of only BC and water-solubles. The mass fraction (f) of each component for each month averaged for 5 years is shown in Figure 2. f_{BC} has an

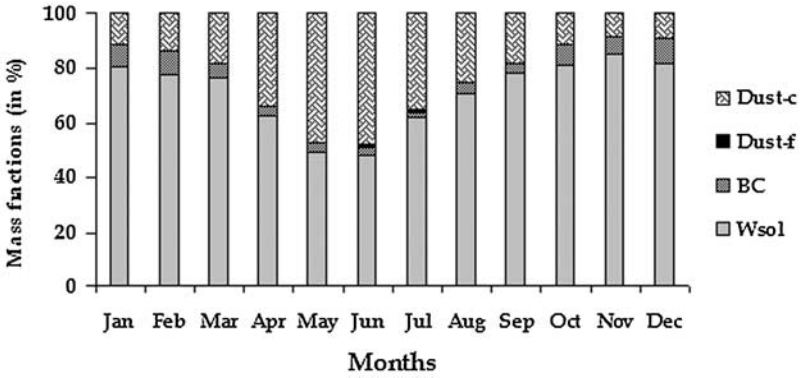

Figure 2. Mass fraction of each component (in %). Each bar represents the value for that particular month averaged for 5 years (for uncertainties, see the text).

uncertainty of ~14% [*Babu and Moorthy*, 2002], whether the f_{dust} (fine + coarse mode) has uncertainty of ~16%. The uncertainty in the mass fractions is based on the measurement uncertainty and the uncertainty due to missing components in the analysis, as the mass fractions are calculated by summing up the mass concentrations of the analyzed components. The mass of wsol components (including the water associated with it) are found to increase linearly with increasing RH up to 70% RH, beyond which the change is exponential. This suggests that at RH higher than 70%, the mass of wsol components are very much sensitive to the change in RH. In the calculations, at RH less than 70%, the uncertainty in the change in mass of wsol due to changes in RH would be ~2% and above 70% RH, it would be ~6%. This would lead to an overall uncertainty of 17–20% in f_{wsol}. f_{BC} varies from a high of ~8% in the winter season to a low ~3% in the monsoon season and f_{wsol} varies from a high of ~80% in the winter season to a low ~50% in the months of May and June, when $f_{dust\text{-}c}$ and f_{wsol} are nearly same. $f_{dust\text{-}f}$ is less than 0.5% on annual scale. The reconstruction of mass of various components is sensitive to RH. If RH decreases, f_{wsol} will reduce, as the water-soluble component is hygroscopic.

2.3. Aerosol DRE Estimation in Clear and Cloudy-Sky Conditions

[15] Aerosol DRE is defined as the effect of aerosols on the net (upward minus downward) radiative fluxes at the surface and at the top-of-atmosphere, the difference being trapped in the atmosphere and transformed into heat energy. Aerosol DRE at both top-of-the-atmosphere (TOA) and surface has been estimated from the difference in radiative fluxes calculated for the aerosol-free and aerosol-laden atmosphere. Aerosols mostly interact with the incoming solar radiation in the shortwave region (SW, 0.25–4 μm), but they also perturb the outgoing longwave (LW, 4–100 μm) radiation budget.

[16] For radiative transfer calculations, we have used Santa Barbara Discrete Ordinate Radiative Transfer (SBDART) model developed by *Ricchiazzi et al.* [1998]. SBDART is a plane-parallel radiative transfer code based on the discrete ordinate approach and has been used by many investigators to estimate aerosol radiative forcing. The radiative transfer equations are numerically integrated with Discrete Ordinate Radiative Transfer (DISORT) module [*Stamnes et al.*, 1988] in the SBDART, which uses a numerically stable algorithm to solve the equations of plane-parallel radiative transfer in a vertically inhomogeneous atmosphere.

[17] The basic input parameters required for the DISORT module in SBDART are spectral AOD, SSA and g. Spectral AOD, SSA and g (in the wavelength range 0.25 to 40 μm) obtained from the optical model have been incorporated in the SBDART model to compute the SW and LW aerosol DRE. Finally the aerosol DRE is estimated as diurnal average following *Dey and Tripathi* [2007]. Surface albedo values are taken from Moderate Resolution Imaging Spectroradiometer (MODIS) surface albedo product (MODIS/Terra Albedo; 16-Day; level-3 Global 1 km SIN Grid). The surface albedo for each month is obtained by averaging the values of each day in that particular month. We have used the columnar water vapor values from AERONET and columnar ozone concentration values from Total Ozone Mapping Spectroradiometer data averaged over each month period. First, the TOA and surface aerosol DRE are estimated for Kanpur region for clear-sky conditions.

[18] Clouds impart an important effect in the solar-climate interaction through reflection (commonly known as "albedo effect"), scattering and absorption. Their presence in the atmosphere, not only induces surface cooling, but also modifies the magnitude and nature of the aerosol forcing in clear-sky condition. Clouds interact with the incoming as well as outgoing radiation and thus alter the radiative balance of the atmosphere. The important cloud parameters that influence the aerosol DRE are the position of the cloud with respect to aerosol, COD, R_{eff} and η. In this analysis, cloudy-sky aerosol DRE (ΔF_{cldy}) at TOA and surface are calculated using the corresponding clear-sky aerosol DRE (ΔF_{clr}) and cloud fraction (η) [*Satheesh et al.*, 2006]:

$$\Delta F_{cldy} = \Delta F_{clr}\,(1-\eta) + \eta \Delta F_{ov}, \tag{2}$$

where ΔF_{ov} is the aerosol forcing in the overcast condition, considering 100% cloud cover (i.e., η = 1). The aerosol DRE in and without the presence of clouds are found to be different, as discussed in section 3.2.

[19] ΔF_{cldy} was parameterized in terms of ΔF_{clr} (equations (3a)–(3d)) and other controlling parameters using the

Table 2. Anthropogenic Efficiency Factors for Surface and Atmospheric Aerosol DRE for Each Month

	Jan	Feb	Mar	Apr	May	Jun	Jul	Aug	Sep	Oct	Nov	Dec
Surface	1.05	1.19	0.97	0.78	0.95	0.97	0.57	0.8	0.94	1.05	1.08	1.09
Atmospheric	1.19	1.52	1.02	0.8	1.17	1.17	0.69	0.84	0.89	1.22	1.11	1.36

values of the cloud optical and microphysical properties obtained for the same period. In these expressions ΔF_{cldy} and ΔF_{clr} are computed using the model-derived aerosol optical properties, as discussed earlier. These parameterizations will help assessing the cloudy-sky aerosol forcing from the clear-sky aerosol forcing and the cloud parameters without running the radiative transfer model in future. The expressions for ΔF_{cldy} for TOA and surface in the SW and LW are given below along with the root mean square error (RMSE) respectively.

$$\begin{aligned} LW_{surface} : \Delta F_{Cldy} &= (0.54661*\Delta F_{Clr}) \\ &\quad - (0.02115*R_{eff}) - (0.02526*\tau_c) \\ &\quad - (0.00293*CTP) - (4.02088*\eta) \\ &\quad + (4.76923*R) + 3.59643, \\ RMSE &= 0.43\ W\ m^{-2}, \end{aligned} \tag{3a}$$

$$\begin{aligned} LW_{TOA} : \Delta F_{Cldy} &= (0.8326*\Delta F_{Clr}) + (0.01392*R_{eff}) \\ &\quad - (0.00366*\tau_c) + (0.00334*CTP) \\ &\quad - (1.60292*\eta) + (5.53623*R) - 3.31403, \\ RMSE &= 0.6\ W\,m^{-2}, \end{aligned} \tag{3b}$$

$$\begin{aligned} SW_{Surface} : \Delta F_{Cldy} &= (0.65548*\Delta F_{Clr}) - (0.00416*R_{eff}) \\ &\quad + (0.38632*\tau_c) - (0.00181*CTP) \\ &\quad + (17.0106*\eta) - (35.30824*R) - 4.10464, \\ RMSE &= 2.66\ W\ m^{-2}, \end{aligned} \tag{3c}$$

$$\begin{aligned} SW_{TOA} : \Delta F_{Cldy} &= (1.02291*\Delta F_{Clr}) - (0.11179*R_{eff}) \\ &\quad + (0.21542*\tau_c) + (0.00903*CTP) \\ &\quad + (14.3935*\eta) - (49.63933*R) + 4.52453, \\ RMSE &= 1.95\ W\ m^{-2}. \end{aligned} \tag{3d}$$

[20] In these expressions, R_{eff} and τ_c are the effective radius and cloud optical depth (COD) of the water/ice clouds, CTP is the cloud top pressure and R is the surface albedo. The cloud parameters are taken from MODIS. MODIS retrieves the cloud optical and microphysical parameters with 1 km spatial resolution using six bands in the visible to infrared region. First, the pixel is tested whether it is suitable for cloud retrieval (i.e., whether the cloud fraction exceeds the detection threshold). Then the appropriate thermodynamic phase is determined (for more details, see *Platnick et al.* [2003] and *King et al.* [1998, 2003]). The data for each pixel (level 2 data) are grouped into $1^\circ \times 1^\circ$ grid with detailed statistical measures to produce level-3 data set, MOD06 [*King et al.*, 2003]. For our computations, if the cloud is low-level cloud (CTP > 680 hPa), the parameters for water phase, for medium-level clouds (680 < CTP < 440 hPa), combined phase and for high-level clouds (CTP < 440 hPa), ice phase have been used [*Doutriaux-Boucher and Sèze*, 1998]. MODIS provides only CTP; hence for cloud bottom pressure (CBP), we have collected data of mixing condensation level (MCL) measured in Chakeri airbase, Kanpur through balloon-sonde. The balloon-sonde was collected twice daily, one in the morning (5.30 local time or 0 GMT) and one in the afternoon (17.30 local time or 12 GMT) to collect information on vertical profiles of temperature, RH and other meteorological parameters. In absence of near real-time data about cloud bottom height, computations were made assuming MCL to be the maximum possible cloud base. The cloud geometrical thickness is deduced from the CTP and CBP for each month. The parameterized equations will help determining the cloudy-sky aerosol DRE over Kanpur using clear-sky aerosol DRE values without running the radiative transfer model.

2.4. Anthropogenic Aerosol DRF

[21] In our estimation of anthropogenic aerosol DRF, we consider BC and water-soluble components as the major anthropogenic species in the region. The water-soluble components in this region comprise mainly $(NH_4)_2SO_4$, NO_3^-, Cl^-, Na^+, K^+ [*Dey and Tripathi*, 2007] and organics. Here it should be mentioned that the estimations are made ignoring any anthropogenic contribution to the dust through land cover changes. Anthropogenic aerosol DRF over Kanpur has been estimated using the anthropogenic AOD_λ, SSA_λ and g_λ, derived from the optical model, as input to the SBDART. A relationship between total aerosol DRF (ΔF) and anthropogenic aerosol DRF (ΔF_A) was established following *Kaufman et al.* [2005]

$$\Delta F_A = \Delta F*AEF*AF, \tag{4}$$

where AEF (anthropogenic efficiency factor) is defined as the ratio of anthropogenic aerosol forcing efficiency to total aerosol forcing efficiency and AF is the anthropogenic fraction. The forcing efficiency can be defined as the forcing per unit optical depth.

[22] The AEF signifies the relative proportion of the anthropogenic aerosol forcing efficiency to the composite aerosol forcing efficiency. AEF values greater than unity (October-February in Table 2) implies higher forcing efficiency for anthropogenic aerosols as compared to that of composite aerosols, which means during this period, the composite aerosol properties are dominated by the anthropogenic components. The values of AEF for each month (Table 2) are derived from the estimated anthropogenic aerosol DRF and composite aerosol DRE for Kanpur region using SBDART. The utility of the AEF is that it can be used to estimate the anthropogenic aerosol DRF in future for this region, if the composite aerosol DRE and AF are known.

Table 3a. Sources of Uncertainties in the Estimates of the Aerosol DRE and Anthropogenic Aerosol DRF

Estimates	Sources of Uncertainties	Uncertainty in Estimates
Aerosol clear- and cloudy-sky DRE	optical properties	10%
Aerosol clear- and cloudy-sky DRE	surface albedo	1.5% [*Dey and Tripathi*, 2007]
Aerosol clear- and cloudy-sky DRE	scale height	5%
Aerosol clear- and cloudy-sky DRE	columnar water vapor	10%
Aerosol clear- and cloudy-sky DRE	columnar ozone	5%
Aerosol cloudy-sky DRE	cloud parameters	10–20%
Anthropogenic aerosol DRF	anthropogenic fraction	6%
Anthropogenic aerosol DRF	cloud parameters	10–20%

ΔF_{TOA} flips sign from negative to positive and sometimes become zero (i.e., surface cooling is compensated by the atmospheric heating). So the AEF values for TOA forcing may be unrealistic and hence we have calculated the AEF values for surface and atmosphere forcing. The anthropogenic TOA aerosol DRE can be estimated from the surface and atmospheric anthropogenic aerosol DRF values.

[23] The critical part of the above equation is AF, as no such measurements exist in IGB. Using these model calculations in conjunction with the satellite data, we suggest a method to estimate the AF for this region. AF represents the relative contribution of the anthropogenic components to the total AOD. The above said relation will enable assessment of the anthropogenic contribution to the total aerosol DRE over Kanpur only if the AF can be known. In absence of any direct measurements, we employ MODIS-aerosol fine mode fraction (AFMF) product to infer the AF. Past studies have utilized MODIS AFMF data to assess the anthropogenic contribution over the oceanic region [*Kaufman et al.*, 2005], as in general, anthropogenic aerosols dominate in the fine mode fraction. The model-derived AF was compared with the MODIS-AFMF product in $1^\circ \times 1^\circ$ grid over Kanpur for the entire 5 year period and a statistically significant relationship was established at 95% confidence level:

$$AF = AFMF*0.65 + 0.1534. \quad (5)$$

The correlation coefficient of the model-derived AF and the MODIS-derived AFMF is 0.96. Comparison of MODIS AFMF product with our model-derived AF reveals that MODIS AFMF product has a bias and needs to be corrected to determine the AF over this region. Thus using the above relation, AF can be estimated and subsequently the anthropogenic aerosol DRF can be assessed for this region. This method of estimation of anthropogenic aerosol DRF has two advantages. First, as AEF is the ratio of two equivalent terms, overall uncertainty will not increase. Second, the AF is validated against the model outputs, which are already matched with ground-based measurements.

2.5. Error Budget of the Aerosol DRE Estimations

[24] While discussing the implications of the temporal variations of radiative forcing due to aerosols, it is important to account for the error budget for such estimations. The source and magnitude of the uncertainties will indicate the present status of the required data and future needs and help in comparing with other estimations globally.

[25] The aerosol DRE has been estimated for Kanpur using the model-derived optical properties in SW and LW wavelength regions. Numerous factors influence the aerosol optical properties and hence the DRE, e.g., size distribution and scale height of each species, state of mixing, RH, chemical composition, surface albedo and sky condition (clouds). Information about individual scale height for each species is not available in the Indian region. Sensitivity study shows that reduction of scale height from 1.2 km to 0.8 km (value reported during INDOEX by *Satheesh et al.* [1999]) reduces $AOD_{0.5}$ by ~10% along with flattening of AOD spectrum. Lower scale height indicates less dispersion of aerosols in the atmospheric column, which leads to overall lower extinction. In that condition, surface aerosol DRE is estimated to be higher by 2 W m^{-2} (than the present case) and TOA aerosol DRE is lower by ~2.6 W m^{-2}. An increase of 20% in the modal radius (R_m) of BC size distribution increases the composite SSA and g (at 0.5 μm) by ~2% and 0.4%, respectively and decreases the composite $AOD_{0.5}$ by 5.8%. This would induce an error of 5% on the TOA and surface DRE estimation. The aerosol optical properties are retrieved with ± 5% error by AERONET; the retrieval error is even less for large AOD [*Dubovik et al.*, 2000]. The uncertainty in BC measurements is ~10% [*Babu and Moorthy*, 2002]. However, the f_{BC} is more important than the absolute mass of BC from the radiative forcing point of view, and measurement uncertainty of f_{BC} is ~14% [*Babu and Moorthy*, 2002].

[26] Table 3a lists the various sources of uncertainties, which lead to the overall uncertainty of various proportions in the estimates of the aerosol DRE (Table 3b). The aerosol DRE estimations require the aerosol optical properties, surface albedo, columnar water vapor and ozone concentration, and aerosol vertical distribution for clear-sky conditions and cloud parameters in addition to those parameters for cloudy-sky condition. The aerosol optical properties depend on the aerosol chemical composition, where we have assumed the organics to be water solubles. This may lead to additional error, but our composite aerosol optical properties are constrained by the AERONET retrievals. While constraining the number concentrations of the individual components by comparison with the AERONET-retrieved AOD spectrum, similar AOD spectrum may arise because of multiple combinations. However, in that case,

Table 3b. Overall Uncertainties in the Estimates of the Aerosol DRF and Anthropogenic Aerosol DRF

Estimates	Overall Uncertainty
Aerosol clear-sky DRE	15%
Aerosol cloudy-sky DRE	20%
Clear-sky anthropogenic DRF	21%
Cloudy-sky anthropogenic DRF	25%

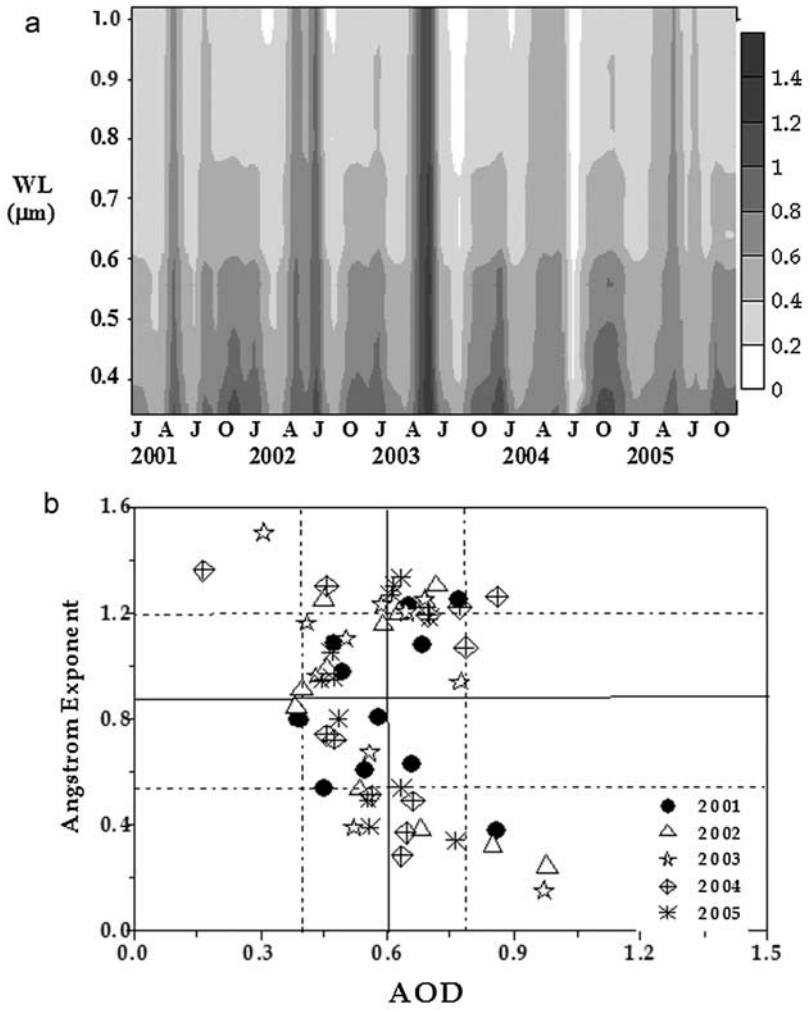

Figure 3. (a) Aerosol optical depth spectrum over Kanpur for 2001–2005 as retrieved by AERONET. J, A, J and O represent January, April, July and October sequentially. (b) Scatterplot between monthly averaged $AOD_{0.5}$ and Angstrom exponent for different years showing the interannual variation in the nature of aerosol loading over Kanpur. The solid lines are the corresponding 5-year means and the dashed lines are the standard deviations.

the resulting SSA and g spectra for each combination would be different. To restrict this possibility, we have matched the model-derived SSA and *g* spectra with the AERONET retrieved SSA and *g* spectra within the retrieval uncertainty, which leads to a unique combination of various individual components that can be the best representative of the composite aerosol optical properties. Thus the model-derived optical properties also exhibit similar uncertainty as of the AERONET retrievals, which are used for radiative transfer calculations for Kanpur region. MODIS-derived surface albedo value can have an average of 6% error in the SW region [*Strahler et al.*, 1999], which will induce ~3.5 and 1.5% error in the estimated TOA and surface forcing, respectively. For anthropogenic aerosol DRF, MODIS AFMF product was corrected after comparing with modeled anthropogenic fraction with 6% uncertainty. As we used AEF, which is a ratio of two similar quantities, the errors in the forcing efficiencies will cancel.

[27] The retrieval error of CTP is 50 hPa for clouds present at more than 3 km height, error being higher for lower clouds [*Platnick et al.*, 2003]. The model uncertainty of R_{eff} is ~0.5 μm for $R_{eff} < 20$ μm. Uncertainty analysis reveals that for COD ~50, error in R_{eff} is less than 0.1 μm, but for optically thin clouds (COD ~1), error in R_{eff} is higher (~0.3 μm). Overall, the retrieval uncertainty is large for smaller values of COD and R_{eff}. The physical uncertainty in R_{eff} is in between 1 and 3 μm for optically thick clouds [*King et al.*, 2003]. Sensitivity study shows COD and cloud fraction (CF) are the two most important parameters influencing the cloudy-sky aerosol forcing. Since, cloudy-sky aerosol DRE is mostly sensitive to COD, large error in R_{eff} does not affect the overall uncertainty much.

[28] The total uncertainty in the estimation of various types of aerosol forcing was then estimated by standard method of error estimation [*Taylor*, 1982]:

$$E_{\Delta F} = \sqrt{\sum_{i=1}^{n} \left(\frac{d(\Delta F)}{dx_i}\right) E(x_i)^2}, \quad (6)$$

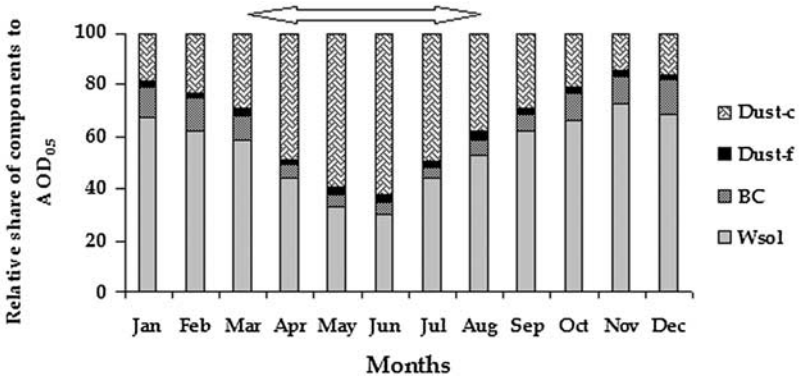

Figure 4a. Relative share of different components to composite $AOD_{0.5}$. Each bar represents the value for that particular month averaged for 5 years. The arrow indicates the period of dust transportation to Kanpur from the arid regions.

where $E_{\Delta F}$ is the error in the estimated forcing, $d(\Delta F)/dx_i$ is the first-order derivative of the forcing with respect to *i*th parameter (x_i) and $E(x_i)$ is the measurement or retrieval error due to *i*th parameter. As shown in Table 3b, the total uncertainty in the estimations of clear-sky aerosol DRE, cloudy-sky aerosol DRE, clear-sky DRF due to anthropogenic fractions and cloudy-sky DRF due to anthropogenic fractions are 15%, 20%, 21% and 25%, respectively. In future, more in situ measurements of various aerosol, cloud and atmospheric parameters in temporal scale are required to minimize this uncertainty. However, with the present status of data set for this region, these estimates are the best to our knowledge.

3. Results

[29] In this section, the important observations made from the temporal heterogeneity of various forcing values over Kanpur are described. First, the key features of aerosol optical properties, derived from the optically equivalent model, are discussed. Then the nature of composite aerosol DRE is discussed followed by anthropogenic aerosol DRF. As the direct effect is significant in the SW portion of the spectrum, the results are mostly shown for SW. However, we have discussed the results about LW forcing whenever appropriate.

3.1. Aerosol Characterization

[30] Model-derived spectral AOD over Kanpur for the 60 months period is shown in Figure 3a. AOD shows strong seasonal variation with reduced spectral dependence during the premonsoon season (March-May) due to enhanced dust loading [*Dey et al.*, 2004]. Mean (± standard deviation) annual AOD at 0.5 μm wavelength for the 5 years, 0.58 ± 0.15, 0.61 ± 0.18, 0.64 ± 0.27, 0.60 ± 0.19 and 0.58 ± 0.10, respectively, signifies very high aerosol loading. Among the 5 years, no significant increasing or decreasing trend is observed in the $AOD_{0.5}$. Although the nature of spectral variation is similar in broader sense, the magnitude of the AOD_λ varies from one year to another. A detailed discussion on interannual variation of aerosol optical properties is beyond the scope of this paper; however it should be pointed out that the low spectral dependence of AOD lasts longer in 2002 and 2003, when dust activities were prolonged. The scatterplot between $AOD_{0.5}$ and α for all the 5 years (Figure 3b) reveals three important features. First, in some months, AOD is nearly equal or more than the 5-year mean, with α nearly equal or lower than the 5-year mean – SD. These months show maximum dust events within the time period and the composite aerosol optical properties are mostly dominated by mineral dust. Secondly, in those months, when AOD is nearly equal or more than 5-yearly mean, with α nearly equal or lower than the 5-year mean + SD, the composite aerosol optical properties are mostly dominated by anthropogenic fine mode aerosols, with insignificant contribution of natural dusts. In rest of the months, the contribution to the composite aerosol optical properties is combined. This indicates that despite being an urban/industrial site in the heart of the IGB, this region has a complex nature of aerosol loading depending on the meteorological conditions.

[31] The relative contribution (RC) of various major components to $AOD_{0.5}$ over Kanpur for each month is shown in Figure 4a. RC_{wsol} in January is as high as 67%, which reduces to mere 30% in June and again builds up to reach 69% in December. RC_{BC} is high in winter months (>11%) and low during the summer months (<6%). $RC_{dust\text{-}f}$ varies between 1 and 3% and $RC_{dust\text{-}c}$ is highest in May and June (>60%). More interesting is the spectral behavior of RC of the components (Figure 4b). RC_{wsol} shows strong spectral decrease, whereas $RC_{dust\text{-}c}$ shows strong spectral increasing trend. RC_{BC} spectrally decreases with varying trend in different seasons. RC_{wsol}, R_{BC} and $RC_{dust\text{-}c}$ in the ultraviolet to near infra red wavelength (0.25 to 1.25 μm), is parameterized in the following form:

$$RC_i(\lambda) = a_i + b_i\lambda, \tag{7}$$

where "a_i" and "b_i" are two coefficients representing the RC_i (0.25 μm) and the rate of change of RC_i with wavelength. $RC_{dust\text{-}f}$ is fitted with second-order polynomial equation:

$$RC(\lambda) = a\lambda^2 + b\lambda + c, \tag{8}$$

as its spectral variation initially increases and then decreases, although this variation is small. Values of "a"

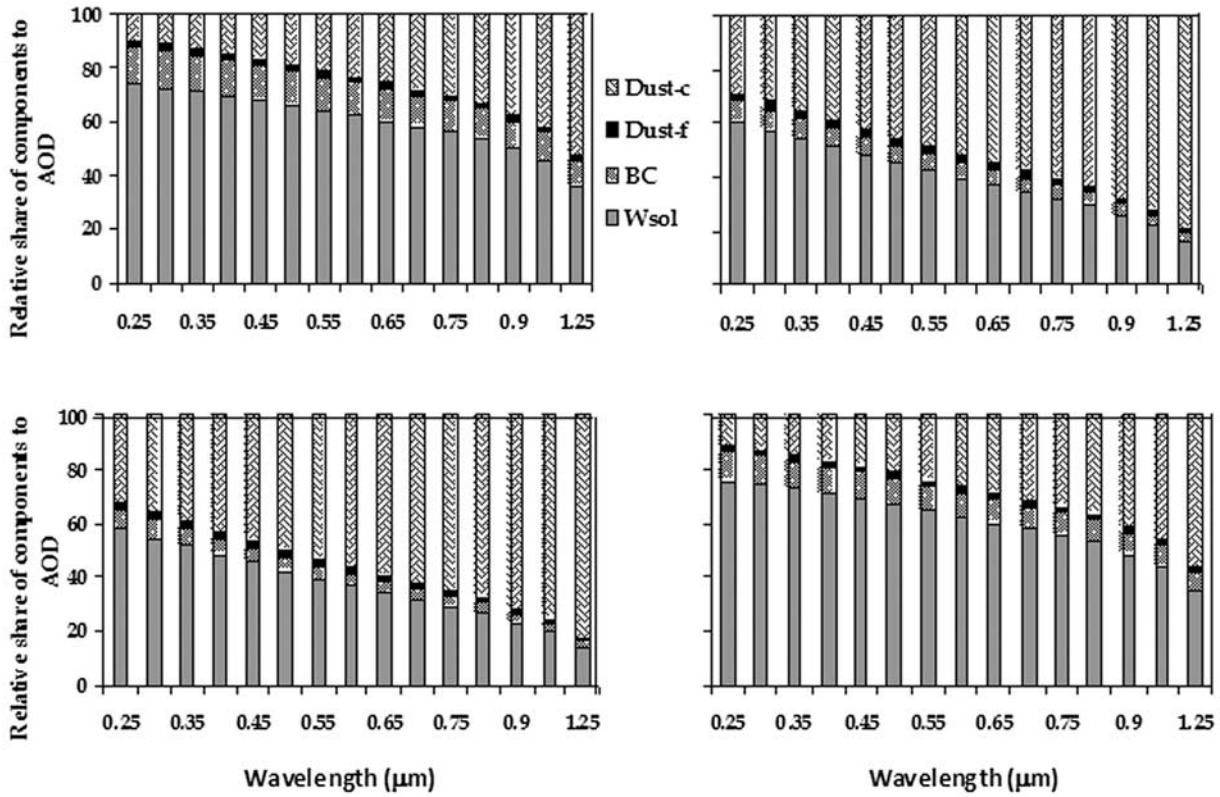

Figure 4b. Spectral variability of relative share of each component to the composite AOD in (top left) winter, (top right) premonsoon, (bottom left) monsoon and (bottom right) postmonsoon seasons.

and "b" for the three components and "a," "b" and "c" for in the four seasons are listed in Table 4.

[32] Besides the AOD, SSA is the most significant parameter influencing the radiative forcing. Throughout the year, SSA (at 0.5 μm) over Kanpur is low (<0.9 for most of the times) because of the presence of absorbing aerosols. However, the spectral variation differs seasonally depending on the relative proportions of the scattering and absorbing components (Figure 4c). In the winter, SSA shows decreasing trend with wavelength, while in the premonsoon season and sometimes in the monsoon, the trend gets reversed. In the postmonsoon season, the variation is mostly spectrally insensitive. Decreasing trend of SSA implies coexistence of scattering water-soluble and absorbing aerosols, as the rate of decrease of scattering coefficient with wavelength is faster than the rate of decrease of absorbing coefficient.

[33] In the condition where dust is the major player, SSA increases with wavelength, as absorption due to dust is much higher at the lower wavelengths and rapidly decreases in the higher wavelengths. The opposing characteristics of wavelength dependence of SSA, i.e., the spectrally increasing and decreasing trends are canceled out in the postmonsoon season leading to least spectral variation, as dust could not influence the optical properties in such extent as compared to that in the premonsoon and monsoon seasons. In the monsoon, some years like 2002 and 2003, when dust activities were prolonged, the variation becomes similar to that in the premonsoon season. Hence maximum interannual variation for SSA spectrum is found for the monsoon season. Decreasing absorption spectrum along with low SSA observed during winter in Delhi [*Ganguly et al.*, 2006] and Kathmandu (in the Himalayan foothills, which is northernmost part of IGB [*Ramanathan and Ramana*, 2005]) from independent measurements supports the fact that the optical properties are not significantly different in the other locations of the IGB.

3.2. Temporal Heterogeneity of Total Aerosol DRE

[34] In this section, the monthly mean climatology and the interannual variations of aerosol DRE in clear-sky

Table 4. Values of "a," "b" and "c" in Winter (December–February), Premonsoon (March–May), Monsoon (June–September) and Postmonsoon (October–November) Seasons

	Winter			Premonsoon			Monsoon			Postmonsoon		
	a	b	c	a	b	c	a	b	c	a	b	c
Wsol	84.42	−38.29		69.13	−46.74		66.1	−46.43		87.59	−42.67	
BC	15.54	−5.36		9.1	−5.22		7.8	−4.97		11.43	−3.74	
$Dust_f$	−2.13	2.87	1.21	−1.7	0.91	2.74	3.74	−10.31	9.42	−2.32	3.05	1.34
$Dust_c$	−2.09	43.83		18.3	53.48		22.59	53.14		−1.35	46.67	

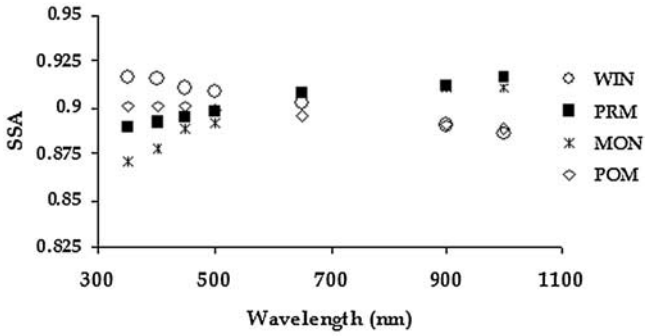

Figure 4c. Spectral variation of SSA as derived by the model in winter (WIN), premonsoon (PRM), monsoon (MON) and postmonsoon (POM) seasons. The values are averaged for 5 years.

(Figure 5a) and cloudy-sky (Figure 5b) conditions over Kanpur are discussed. In the following discussions, aerosol DRE will be referred to as forcing for sake of brevity. The annual mean ± SD (ranges given within brackets) TOA, surface and atmospheric clear-sky forcing over Kanpur are −4.1 ± 6 (−19.6 to +6.1), −31.8 ± 10.9 (−5.8 to −62.3) and +27.7 ± 10.4 (+11.6 to +63) W m^{-2}, respectively. The corresponding cloudy-sky forcing values are +1.4 ± 6.1 (−10.2 to +16.6), −23.3 ± 9.3 (−3.5 to −43.8) and +24.8 ± 9.7 (+5.4 to +51.8) W m^{-2}, respectively. Clear-sky forcing reveals three major points. First, large negative surface forcing (more than −20 W m^{-2}) was observed in all the months with two peaks, one during the winter and the other during the premonsoon when the surface forcing exceeds −30 W m^{-2}. Secondly, TOA forcing was close to zero in January, July and September, negative in other months except August when TOA forcing flips to positive sign. Thirdly, very high atmospheric heating persists throughout the year. The surface cooling in the SW is compensated maximum up to 11% by LW surface heating in the summer months. However, LW atmospheric forcing close to zero (i.e., the TOA and surface LW forcing cancel out each other) in most of the months except monsoon season (>1.5 W m^{-2}) indicate that the atmospheric heating is negligible in the LW region.

[35] In presence of clouds, mean annual TOA forcing switches from cooling to heating, while the surface forcing becomes less negative. This has compensated the excess heating at TOA maintaining the atmospheric heating almost similar to the clear-sky condition. The reduction in magnitude of the negative surface forcing in cloudy-sky condition is high (more than 10 W m^{-2}) during the December-January and May-July. In these months, TOA forcing also increases by more than 7 W m^{-2}. In the winter and summer months, clouds over Kanpur are mostly stratocumulus with high optical depth. During the winter, as most of the aerosols are confined within the boundary layer, they get lesser chance to interact with the incoming solar radiation, a major part of which is reflected back to the space by optically thick clouds. Hence the surface cooling due to aerosols reduces and TOA forcing flips toward positive side indicating warming effect.

[36] The temporal variations of aerosol forcing in clear and cloudy-sky forcing are shown in Figures 5c and 5d. It is interesting to note that the monthly variations of aerosol forcing over Kanpur in each year are not uniform. For example, in 2003, the dust activity was the most intense, but the aerosol loading decreased very sharply after June, when monsoonal rain started, resulting in lowest aerosol surface DRE. In August, the absolute magnitude of surface DRE is low because of the smallest aerosol loading; hence the relative change in surface forcing due to inclusion of cloud

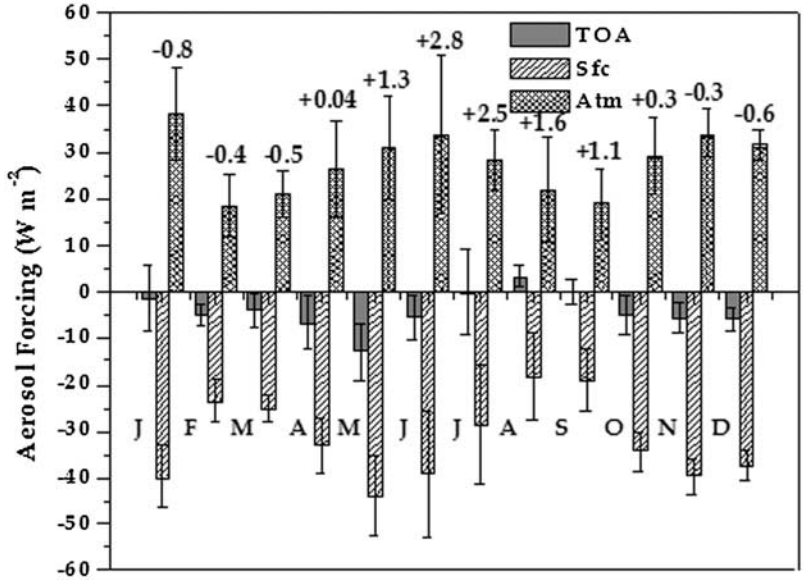

Figure 5a. Clear-sky aerosol DRE over Kanpur at TOA, surface (Sfc) and atmosphere. Each column is the monthly mean value for 5 years (2001–2005), and the vertical bars are the corresponding standard deviations. The values above the atmospheric forcing column are the corresponding mean LW atmospheric forcing.

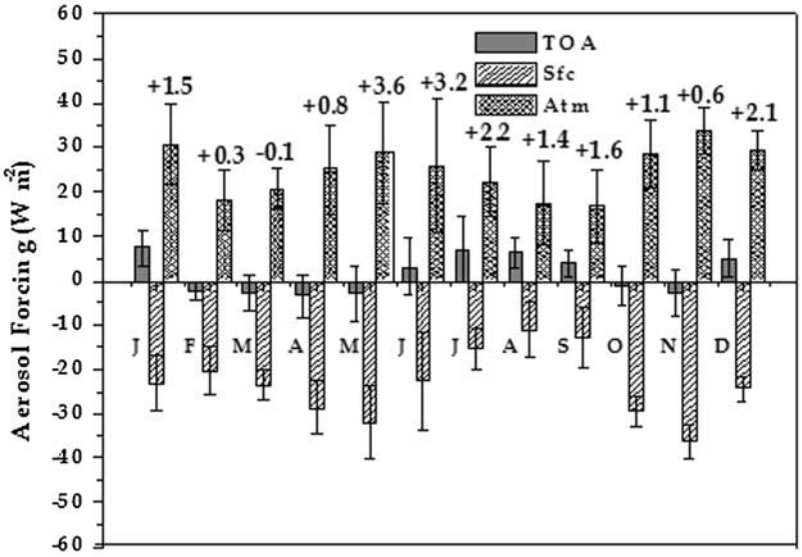

Figure 5b. Same as Figure 5a but for cloudy-sky conditions.

is also less. In other months, as the cloud fraction is low (<0.3), the effect is not so conspicuous. In the LW region, however, the atmospheric forcing increases because of more interaction of clouds with the LW radiation. The sensitivity of the aerosol surface forcing to the various cloud parameters are tested to find the most influential cloud parameter in reduction of aerosol surface forcing. Each cloud parameter was linearly correlated to the difference between the aerosol surface forcing estimates in clear and cloudy-sky and the rate of change of aerosol surface forcing per 10% change in cloud parameters are summarized in Table 5. The cloud fraction emerges the most important parameter. For same cloud fraction, higher-level clouds will cause higher reduction in surface cooling than low-level clouds. Again, brighter clouds (i.e., having higher COD) will cause larger reduction in aerosol surface forcing. The brightness or reflectivity of clouds is affected by aerosol properties (i.e., the indirect effect) and the formation of clouds at certain altitude is affected by meteorology. Hence both will govern the role of clouds on affecting the aerosol direct radiative effects. There is one study done on the aerosol indirect effect in the IGB [*Tripathi et al.*, 2007a], where the intensity of aerosol indirect effect is shown to be pronounced in the winter season, while in the other seasons, the role of meteorology cannot be overlooked. From our analyses, it can be commented that the presence of clouds alter the aerosol DRE quite significantly depending on their macrophysical and microphysical properties, which in turn depend on the aerosol properties and the meteorology. However, many more studies are actually required before drawing any quantitative conclusions.

[37] The monthly variations in the aerosol forcing values are evident, with maximum intra-annual variation occurring in the year 2004. The yearly averaged cloud fraction and its temporal pattern in the 5 years are similar. However, in the years 2003 and 2004, the cloud fractions in the winter are higher than that in the other years. Again, in the year 2005, the cloud fraction in the monsoon season is relatively lower than the previous years. Unlike the Indian Ocean, the SW atmospheric aerosol forcing over Kanpur in cloudy-sky condition most of the time decreases as compared to the clear-sky atmospheric aerosol forcing with exception in few months. However, in the LW region, the effect is found to be reversed. Both the TOA and surface forcing are positive in clear-sky condition, leading to a very small cooling effect in the atmosphere sometimes. When cloud parameters are incorporated, the surface forcing is reduced at a much higher rate than the TOA forcing, and hence the atmospheric absorption increases. This effect is found to be more conspicuous when the low-level clouds are present. However, no statistically significant trend is found for the aerosol forcing in these 5 years.

[38] The total aerosol surface forcing is partitioned to investigate the contribution of individual components to the aerosol DRE in this region (Figure 6). The monthly variations of RC of various components to DRE are different from the variations of their mass fractions or RC to AOD. RC_{BC} varies from a high of ~56% in the winter to a low of ~19% in May. On an annual basis, ~5% BC mass fraction (f_{BC}) contributes ~9% to total $AOD_{0.5}$, but ~40% to the total aerosol surface forcing. Water-soluble components contribute to ~20% to the annual surface forcing, and the contribution is almost similar throughout the year except in June (~10%). $RC_{dust\text{-}f}$ is lower than 2% for all the months. Annually, $RC_{dust\text{-}c}$ is 29% to the total aerosol mass, 34% to $AOD_{0.5}$ and 39% to the total surface forcing. $RC_{dust\text{-}c}$ to total surface forcing is more than 55% during April-July and less than 20% during November to February. RC of various components clearly indicates that BC is the most crucial player in the aerosol surface forcing for this region. Higher absorption of incoming solar radiation by BC as compared to the other components lead to higher RC of BC to composite aerosol surface forcing. RC_{BC} to the total aerosol surface forcing during the INDOEX was found to be ~35% [*Podgorny et al.*, 2000], which is 1.6 times less than the wintertime value in Kanpur.

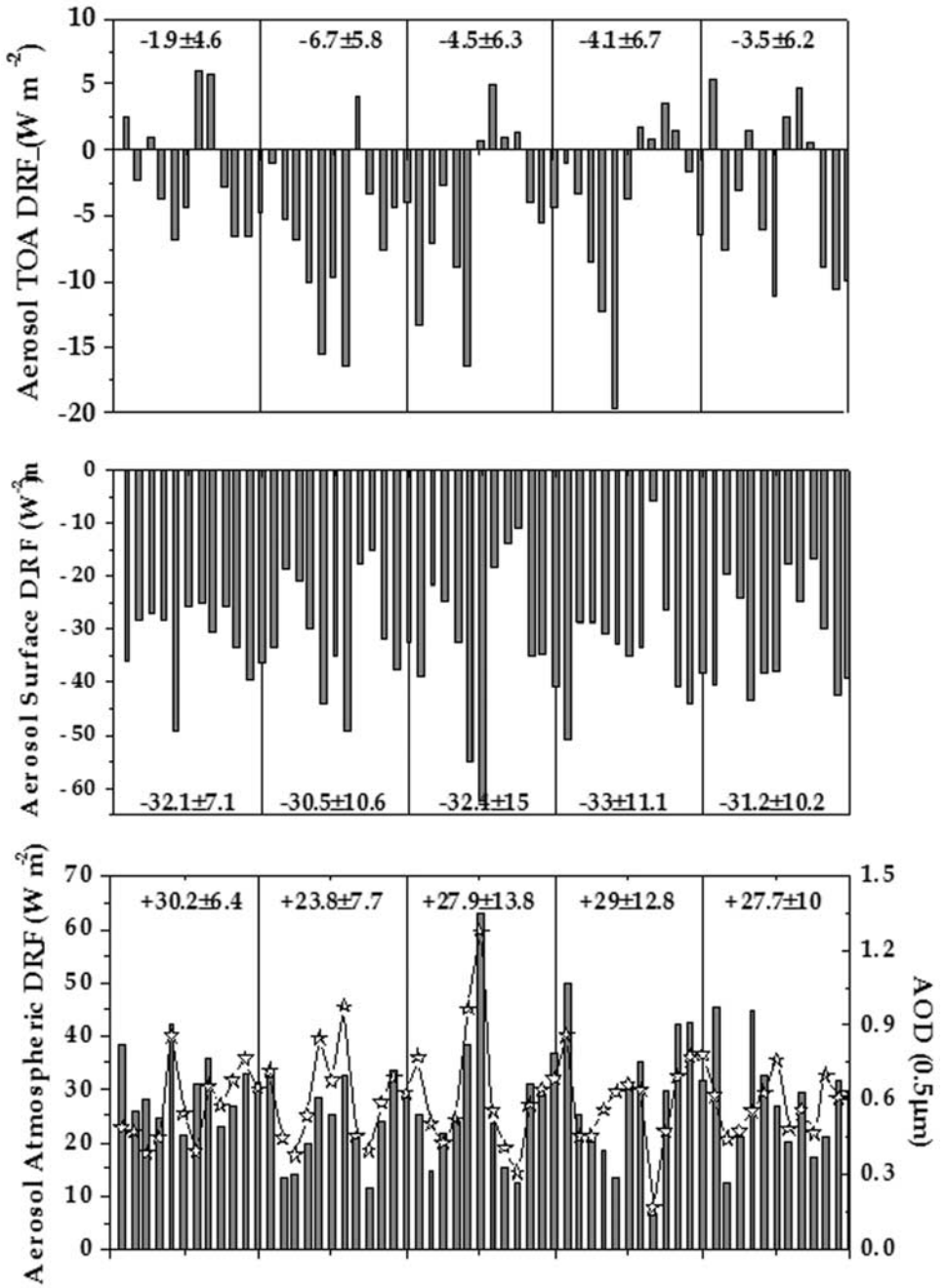

Figure 5c. Temporal variation of monthly averaged TOA, surface and atmospheric clear-sky SW aerosol DRE along with $AOD_{0.5}$ (bold line with stars) in Kanpur shown as monthly averages. The annual average (±SD) values are written in each box (starting from 2001 on the left to 2005 on the right).

3.3. Anthropogenic Contribution to the Aerosol DRE

[39] In this section, the temporal variability of aerosol forcing due to anthropogenic fraction over Kanpur are discussed with the term "anthropogenic forcing" used for "anthropogenic aerosol DRF" for sake of brevity. Monthly mean SW anthropogenic and natural (total minus anthropogenic) forcing at surface over Kanpur are shown in Figure 7a. The anthropogenic surface forcing contributes to more than 80% of total aerosol surface forcing from October to February. Anthropogenic surface forcing starts decreasing from March onward, and from April, natural forcing overtakes the anthropogenic forcing. The relative proportion of anthropogenic forcing to total forcing is lowest (29%) in the month of July. The annual mean ±SD (ranges within brackets) TOA, surface and atmospheric clear-sky anthropogenic forcing over Kanpur are +0.3 ± 2.5 (−2.4 to +4.8), −19.9 ± 9 (−8.5 to −34.3) and +20.2 ± 9.9 (+10.9 to +38.6) W m^{-2}, respectively. The most striking observation is that if only anthropogenic aerosols are considered, TOA forcing increases by a large margin. The corresponding cloudy-sky forcing values are +2.4 ± 4.3 (−1.9 to +11), −16.7 ± 8.1 (−5.7 to −31.1) and +19.1 ± 9.7 (+9 to +34.3)

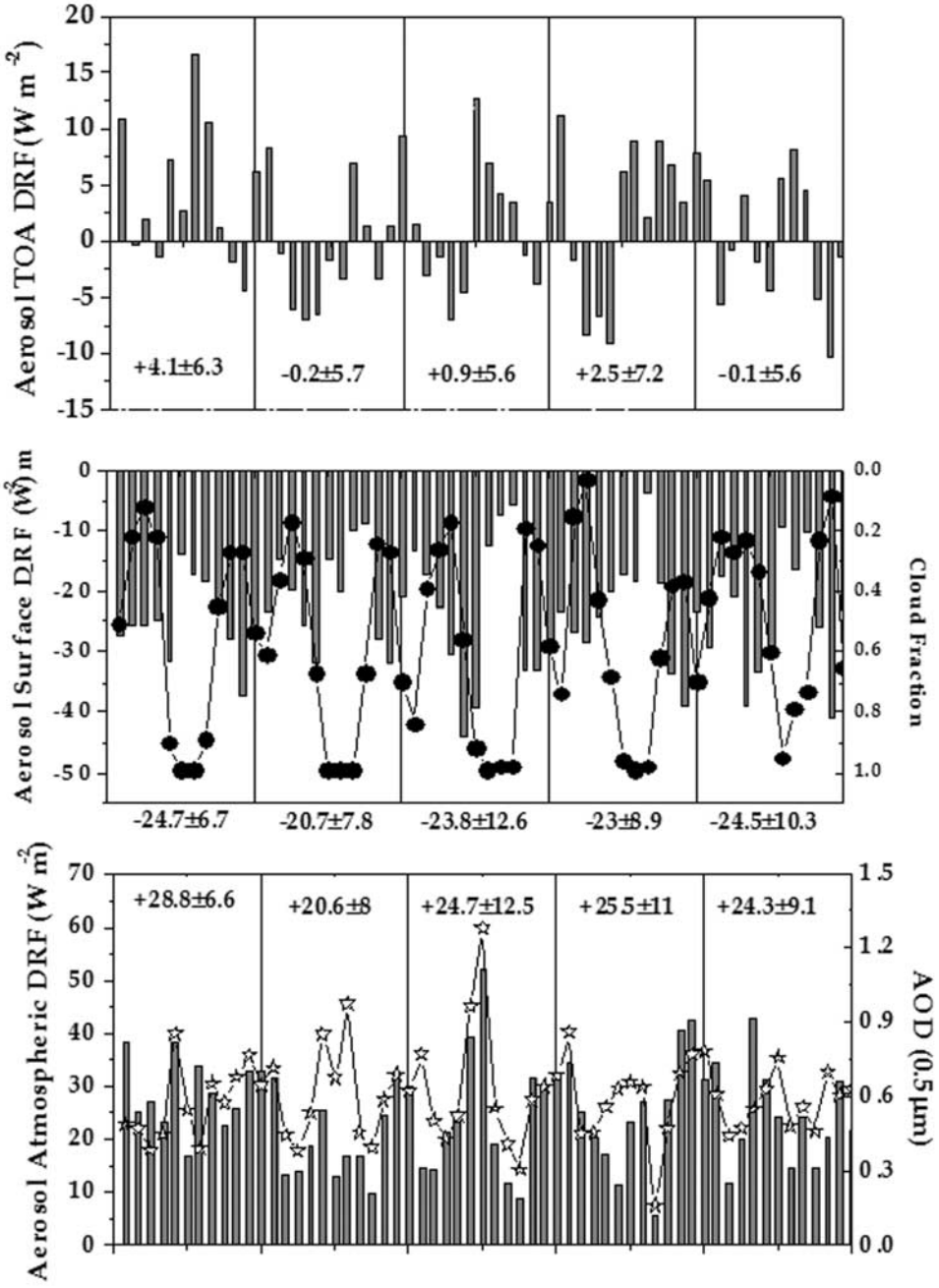

Figure 5d. Same as Figure 5c but for cloudy-sky conditions. The bold line with solid circles indicates the cloud fraction for the corresponding month.

W m^{-2}, respectively. Similar to total forcing, inclusion of clouds increases the TOA forcing, which balances the reduction of the surface forcing for most of the months (Figure 7b). However, in the monsoon season and in January, the atmospheric forcing in cloudy-sky condition decreases by more than 10% as compared to clear-sky condition. The mean annual contribution of the anthropogenic surface and atmospheric forcing to the total surface and atmospheric forcing over Kanpur is 63% and 71% respectively.

[40] The temporal variations of the TOA, surface and atmospheric anthropogenic forcing over Kanpur in SW are shown in Figure 7c. Unlike the total aerosol forcing, the

Table 5. Influence of Various Cloud Parameters in Affecting the Aerosol Surface DRE

Parameter	Correlation Coefficient	Significance Level	Rate of Change of Aerosol Surface Forcing (in %) for 10% Change in Cloud Parameter
Cloud fraction	0.92	99%	49.8 ± 2.9
COD	0.52	99%	1.7 ± 0.4
R_{eff}	0.05	insignificant	−0.19 ± 0.5
CTP	0.51	99%	−0.06 ± 0.01

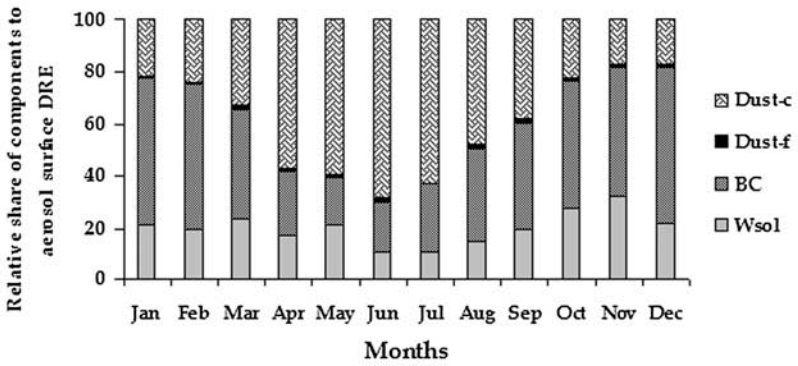

Figure 6. Relative proportions of each component to the aerosol surface DRE.

anthropogenic forcing at surface and atmosphere show a low from March to September, when the aerosol optical properties in Kanpur is dominated by natural dusts. The TOA and surface anthropogenic forcing are higher in the years 2001 and 2004, because of higher BC concentration in these years as compared to other years. The anthropogenic contribution to the total aerosol atmospheric heating is found to be least in the year 2003, when the dust activities were prolonged as discussed earlier. The positive TOA forcing in summer months is due to enhanced absorption of radiation reflected back by brighter surface (i.e., high albedo). The 2003–2004 and 2004–2005 winter seasons show highest atmospheric heating (> 35 W m^{-2}) due to anthropogenic aerosols. The contribution of anthropogenic aerosols to total surface forcing varies in a wide range of 18–95%, with minimum contribution in the years of 2003 and 2005.

4. Discussions and Implications to Regional Climate

[41] So far, only the temporal variability of the aerosol DRE over Kanpur region has been discussed. However, how do these values compare with the aerosol DRE estimated over other regions in India and oceanic regions around the Indian subcontinent? Are these values high if compared to the other polluted regions? To seek these answers, a comparative study is made with the available estimates from literature. Various regions characterized by different kind of sources are considered to have better understanding of the aerosol radiative effect on the global climate. The aerosol DRE values of Kanpur are compared with the estimates made for other polluted cities in India and urban areas in the IGB (Table 6).

[42] In India, besides Kanpur only in Ahmedabad, aerosol DRE has been estimated throughout the year. Ahmedabad shows higher atmospheric absorption on annual scale, but the wintertime atmospheric absorption due to aerosols is lower than the Kanpur value. In Delhi, the surface and atmospheric aerosol DRE are higher than those in Kanpur because of higher aerosol concentration. In the high-altitude sites in the foothills of Himalaya, Nainital and Kathmandu, although the absolute values of surface aerosol DRE are low, the forcing efficiencies are close to those in the regions in IGB. The aerosol DRE in IGB sites, Delhi and Kanpur

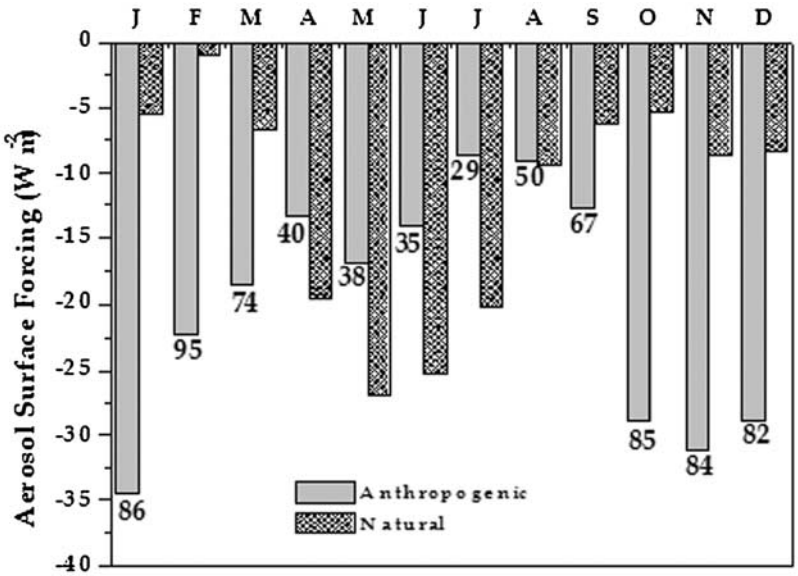

Figure 7a. Clear-sky anthropogenic and natural aerosol surface DRF over Kanpur. The values written below each column are the relative percentage contribution of anthropogenic aerosols to aerosol surface DRE.

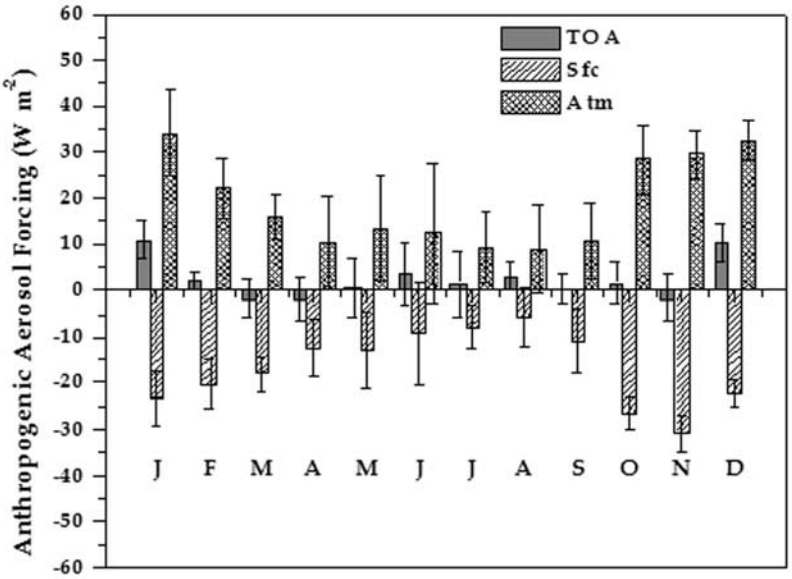

Figure 7b. Cloudy-sky anthropogenic aerosol DRF at TOA, surface and atmosphere over Kanpur. Each column is the monthly mean for 2001–2005, and the corresponding error bars are the standard deviation.

show higher values as compared to the other urban areas in India and adjacent oceans. This high atmospheric absorption in the IGB is due to the higher f_{BC} and the mixing of BC with dust in the summer leading to high TOA DRE. The geographic location, favorable meteorological condition and continuous source of anthropogenic aerosols throughout the year in association with natural dust transported from arid regions in the west make the IGB a region of concern in terms of aerosol radiative effects. The persistence of the aerosols in the basin is affecting the regional climate no doubt; the implications are discussed in the next section.

4.1. Atmospheric Heating

[43] High net (SW + LW) atmospheric heating implies that the excess energy in this region is trapped in the atmosphere. The heating rate of the atmosphere is defined as [*Liou*, 2002]:

$$\frac{\partial T}{\partial t} = \frac{g}{C_p}\frac{\Delta F_{atm}}{\Delta P}, \tag{9}$$

where $\partial T/\partial t$ is the heating rate, C_p is the specific heat capacity of air at constant pressure, ΔF_{atm} is the atmospheric heating, g is the acceleration due to gravity and ΔP is the atmospheric pressure. The difference in clear-sky and cloudy-sky heating rate is insignificant at 95% confidence level because of the fact that the reduction of surface forcing is compensated by increase in TOA forcing in the presence of clouds. The mean (±SD) annual clear-sky atmospheric heating rate over Kanpur is 0.84 ± 0.3 K d^{-1}, which is 68% higher than the corresponding wintertime value for the Indian Ocean [*Satheesh et al.*, 2002]. The heating rate is highest during December-January and May-June ($\sim$ 1 K d^{-1}), because of strong atmospheric absorption. The winter months have the highest concentration of absorbing BC, whereas in May, moderately absorbing dust often gets mixed with BC [*Dey et al.*, 2005] resulting in high atmospheric heating. The anthropogenic fraction is responsible for 67.6% to the heating rate observed over Kanpur region.

4.2. Possible Impact on the Regional Climate

[44] The most important implication for such high negative surface forcing is the persistent large reduction of direct solar radiation in the IGB. Presence of clouds decrease the surface cooling to some extent, but they themselves induce large cooling, 2–3 times higher than the clear-sky condition. On an average, aerosols reduce the net solar radiation at the surface over the Kanpur region by 17%. The INDOEX observations have shown that the large surface cooling and atmospheric heating affect the regional hydrological cycle [*Ramanathan et al.*, 2001b]. As most of the aerosols are concentrated in the lower atmosphere, that too within the first few km, atmospheric heating is most effective in this region.

[45] Now the question is that how the regional climate reacts to this large reduction in irradiance. The climate system maintains a balance at surface between surface radiation, latent heat flux and sensible heat flux. Ignoring other anthropogenic influences on the hydrological cycle for the sake of isolating regional aerosol effects, either latent heat flux or sensible heat flux or both would decrease to maintain the radiative balance due to loss of surface irradiance. The loss in latent heat flux implies reduction of surface evaporation [*Roderick and Farquhar*, 2002], which would consequently reduce the moisture content of the atmosphere and the regional hydrological cycle would be effectively spun down [*Ramanathan et al.*, 2001a]. It seems to be a paradox that observations indicate decreasing evaporation in global scale despite the increment in surface temperature due to global warming. However, *Roderick and Farquhar* [2002] have shown that the evaporation is much more sensitive to the surface radiation balance, which is decreasing because of aerosols and clouds. One earlier study by *Chattopadhyay and Hulme* [1997] using long-term data

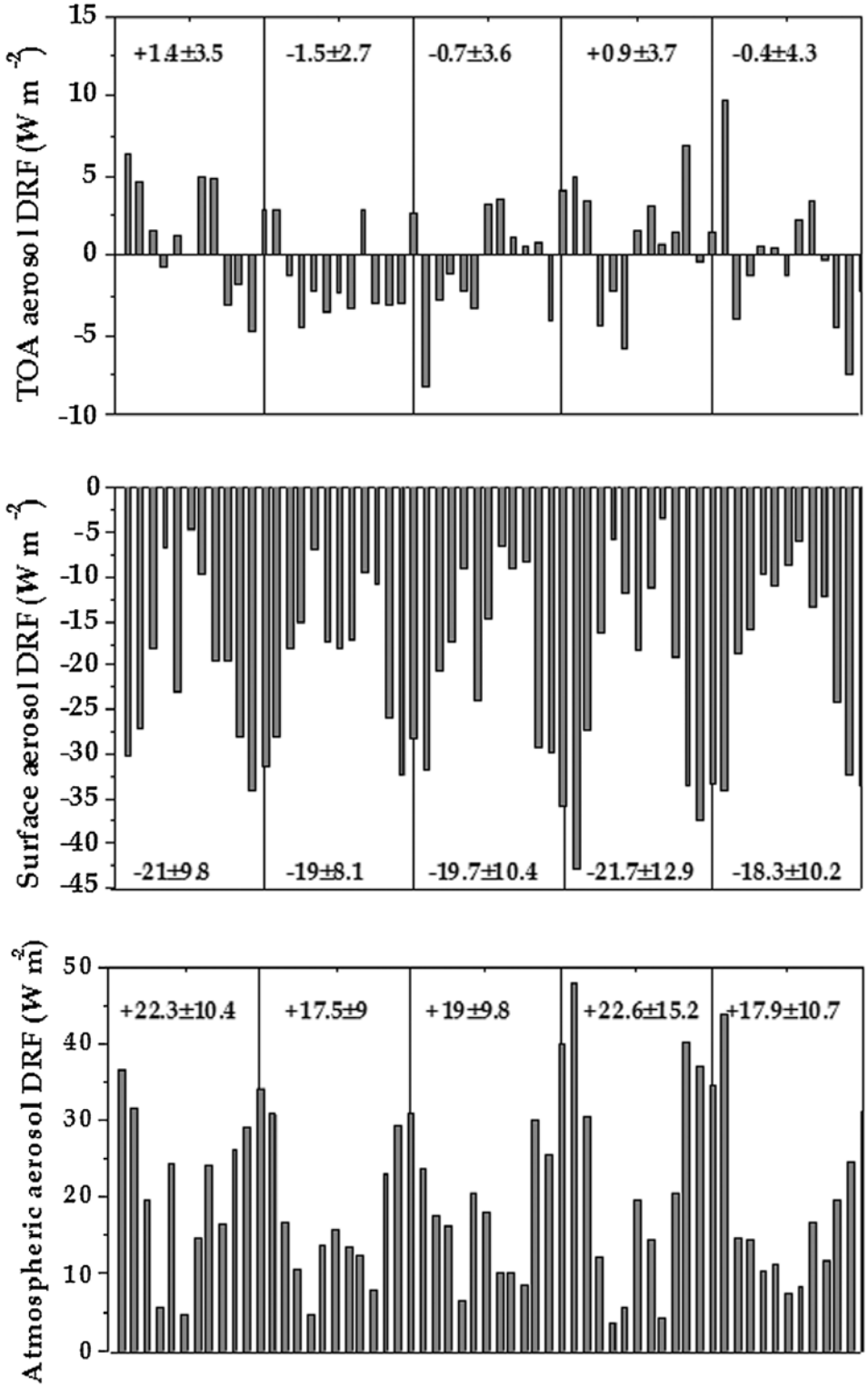

Figure 7c. Interannual variations of anthropogenic aerosol clear-sky TOA, surface and atmospheric DRF over Kanpur in SW with the mean (±SD) annual value shown in each box (starting from 2001 on the left to 2005 on the right).

over India showed that the evaporation in Delhi has decreased during the 1960–1992 period. Also, *Ramanathan and Ramana* [2005], using the aerosol measurements at Kathmandu (in the foothills of Himalaya) and projecting their results for the IGB, have found that during the dry season (October–May) the boundary layer humidity increased by ~5–10% because of strengthening of low-level inversion. They have also found that the pan evaporation data at Kathmandu showed a decrease by ~9 W m^{-2} from 1976–1986 to 1996–2000 periods, which accounts for

Table 6. Comparison Between Aerosol Surface/Atmospheric DRE Estimations for Kanpur and Other Urban Locations in India[a]

Cities	Location	Surface/Atmosphere	Period (comments)	Reference
Kanpur	26.47°N, 80.33°E	−31.8/+27.7	annual (urban)	this paper
Kanpur	26.28°N, 80.20°E	−33.6/+29.4	winter (urban, clear-sky)	this paper
Delhi	28.38°N, 77.17°E	−51/+52	winter (urban, clear-sky)	*Ganguly et al.* [2006]
Hissar	27.17°N, 77.58°E	−21/+20	winter (semiurban, clear-sky)	*Ramachandran et al.* [2006]
Nainital	25.25°N, 81.58°E	−4.2/+0.7	winter (high altitude)	*Pant et al.* [2006]
Kathmandu	25.22°N, 83°E	−25/+25	winter (high altitude)	*Ramana et al.* [2004]
Ahmedabad	23.05°N, 72.55°E	−49/+43.6	annual (urban)	*Ganguly and Jayaraman* [2006]
Ahmedabad	23.05°N, 72.55°E	−54/+28	winter	*Ganguly and Jayaraman* [2006]
Pune	18.32°N, 73.51°E	−33/+33	Nov–Apr (urban)	*Pandithurai et al.* [2004]
Bangalore	13°N, 77°E	−23/+28	Oct–Dec (urban)	*Babu et al.* [2002]
Hyderabad	17°N, 78°E	−33/+42	Jan–May (urban)	*Badarinath and Latha* [2006]
Chennai	13.04°N, 80.17°E	−19/+13	Feb–Mar (urban)	*Ramachandran* [2005]
Central India	multiple stations	−15 to −40	Feb (urban and rural)	*Ganguly et al.* [2005]
South India	multiple stations	∼−27.5/+22	Feb 2004, SW clear-sky	*Jayaraman et al.* [2006]
Pune	18.32°N, 73.51°E	−33/+33	Nov–Apr (urban)	*Pandithurai et al.* [2004]
Arabian Sea		−27/+15	Mar–Apr (polluted marine)	*Moorthy et al.* [2005]
Bay of Bengal		−27/+23	Mar (polluted marine)	*Satheesh* [2002]
Indian Ocean		−29/+19	Feb–Mar (polluted urban)	*Satheesh et al.* [2002]

[a]All the values are in W m^{-2}.

nearly 30% of the estimated surface solar irradiance reduction. The remaining amount is balanced by decrease in sensible and latent heat fluxes and enhanced back radiation from the warmer atmosphere. The aerosol loading in India has also increased drastically in the last 30 years [*Ramanathan and Ramana*, 2005; *Massie et al.*, 2004]. Analysis of TOMS data suggests that during the winter season (when anthropogenic aerosols dominate the composite optical properties), aerosol loading has increased at $10.6 \pm 4.9\%$ $decade^{-1}$ rate in India [*Massie et al.*, 2004]. It means if the aerosol burden, and more precisely the absorbing BC, increases at similar rate, present-day radiative forcing would also increase at even faster rate, as it would increase the forcing efficiency and that would severely affect the regional hydrological cycle.

[46] To summarize this effect, the warmer atmosphere close to surface (i.e., high atmospheric heating) and colder surface due to large negative cooling would create an environment where energy flow from Earth's surface to atmosphere would be suppressed. This would increase the low-level inversions and strengthen the boundary layer stability. In the IGB, the large reduction of solar irradiance persists spatially as well as temporally, as indicated by this paper and some recent studies, which suggests that the effect is regional, not local, and the climate would not get enough time to readjust to its original state, if similar condition persists for long in the future. Even in the monsoon season, the surface cooling remains high. Further studies are needed to address this serious issue in detail for this region, as the monsoon is most important natural phenomenon influencing the region's economy.

[47] Another climatic issue is the indirect effect of aerosols in this region. Such high aerosol loading could change the cloud microphysical properties. Although there are no measurements of cloud condensation nuclei and ice nuclei for this region, satellite data suggests a decrease of effective radius for both water and ice clouds in large area [*Tripathi et al.*, 2007a], which will further affect the precipitation. Reduced cloud effective radius and high concentration of absorbing aerosols would effectively increase the cloud lifetime [*Menon et al.*, 2002], which in turn would increase the surface cooling, thus regulating a positive feedback. This aspect also needs to be investigated with in situ measurements.

5. Conclusions

[48] The temporal heterogeneity of the aerosol DRE and the anthropogenic aerosol DRF are investigated over the Kanpur region in the IGB for the time period of 2001–2005 on the basis of the measured aerosol chemical composition for a short period of time and the measurements of aerosol optical and physical properties for longer (5 years) period of time. The major conclusions from this study that come out are the following:

[49] 1. The optically equivalent model reveals that the aerosol DRE in Kanpur region shows strong seasonal variation due to seasonal changes in the aerosol loading. The relative contribution of water-soluble scattering components to AOD varies in the range of 30% (in the premonsoon season characterized by dust loading) to 68% (in winter) with the relative contribution showing a decrease with increasing wavelengths. BC contributes 5–14% of AOD with the relative contribution showing very slight decrease with increasing wavelengths. Contribution of dust to AOD reaches a maxima peak (>55%) in May-June and a minima (<20%) from November to January and exhibits increasing trend with increasing wavelengths. For most of the times, $SSA_{0.5}$ remains less than 0.9, but as the individual components show different spectral trends, the composite SSA spectrum depends on the relative proportions of the components.

[50] 2. Annual mean (±SD) SW clear-sky aerosol DRE at TOA, surface and atmosphere over Kanpur are estimated to be -4.1 ± 6, -31.8 ± 10.9 and $+27.7 \pm 10.4$ W m^{-2}. The large negative surface forcing in the SW is partially (up to 11%) compensated by LW heating. Inclusion of clouds reduces the surface cooling by more than 10 W m^{-2} in December-January and May-July. However, the reduction is balanced by the enhancement in TOA forcing. The corresponding SW cloudy-sky DRE values are $+1.4 \pm 6.1$, -23.3 ± 9.3 and $+24.8 \pm 9.7$ W m^{-2}, respectively. The

aerosol DRE is found to be highest in the year 2004 and lowest in 2002.

[51] 3. RC_{BC} to the aerosol surface DRE varies from a high of ~56% in the winter to a low of ~19% in May. Water-solubles and $dust_f$ contribute to ~20% and less than 2% to the annual aerosol surface DRE, and the contribution is quite uniform throughout the year. BC seems to be the most crucial player in this region. On an annual basis, ~5% f_{BC} contributes ~9% to total $AOD_{0.5}$, but ~40% to the aerosol surface DRE. Annually, $RC_{dust\text{-}c}$ is 29% to the total aerosol mass, 34% to $AOD_{0.5}$ and 39% to the total surface DRE.

[52] 4. Anthropogenic aerosols contribute to more than 80% of the aerosol surface DRE during October to February. The relative contribution of natural aerosols to DRE due to transportation of dusts starts increasing from March reaching maxima of 71% in July. The annual mean (±SD) TOA, surface and atmospheric clear-sky anthropogenic aerosol DRF over Kanpur are $+0.3 \pm 2.5$, -19.9 ± 9 and $+20.2 \pm 9.9$ W m^{-2}, respectively. The anthropogenic aerosol DRF is highest in the years 2001 and 2004 because of higher BC concentration.

[53] 5. Large negative surface forcing and positive atmospheric forcing in the Kanpur region raise several climatic issues. The atmosphere is getting heated by more than 1 K d^{-1} in the winter and premonsoon seasons because of highest atmospheric absorption. Anthropogenic aerosols contribute 65.4% to the mean (±SD) annual heating rate of 0.84 ± 0.3 K d^{-1} over Kanpur. Persistently large reduction of net surface solar radiation would affect the radiative balance at the surface by decreasing either the latent heat flux through suppressed evaporation or sensible heat flux or both. Such large aerosol loading in the atmosphere would also alter the cloud microphysics through indirect effect. Hence there is a need to understand the effect of the aerosols on the regional hydrological cycle in much better way, which would require more in situ measurements to reduce the present-day uncertainty of the radiative forcing.

[54] **Acknowledgments.** This work is financially supported through a research project under the DST-ICRP program. The efforts of PIs of Kanpur AERONET site are appreciated. We are thankful to Prashant Torai, Wing Commander (Met.) of Chakeri Air Base, Kanpur, for providing the radiosonde data. We are grateful to the anonymous reviewers which help us in improving the manuscript.

References

Auffhammer, M., V. Ramanathan, and J. R. Vincent (2006), Integrated model shows that atmospheric brown clouds and greenhouse gases have reduced rice harvests in India, *Proc. Natl. Acad. Sci. U. S. A.*, *103*(52), 19,668–19,672.

Babu, S. S., and K. K. Moorthy (2002), Aerosol black carbon over a tropical station in India, *Geophys. Res. Lett.*, *29*(23), 2098, doi:10.1029/2002GL015662.

Babu, S. S., S. K. Satheesh, and K. K. Moorthy (2002), Aerosol radiative forcing due to enhanced black carbon at an urban site in India, *Geophys. Res. Lett.*, *29*(18), 1880, doi:10.1029/2002GL015826.

Badarinath, K. V. S., and K. M. Latha (2006), Direct radiative forcing from black carbon aerosols over urban environment, *Adv. Space Res.*, *37*(12), 2183–2188.

Bates, T. S., et al. (2006), Aerosol direct radiative effects over northwest Atlantic, northwest Pacific, and north Indian Oceans: Estimates based on in-situ chemical and optical measurements and chemical transport modeling, *Atmos. Chem. Phys.*, *6*, 1657–1732.

Chattopadhyay, N., and M. Hulme (1997), Evaporation and potential evapotranspiration in India under conditions of recent and future climate change, *Agric. For. Meteorol.*, *87*, 55–73.

Chinnam, N., S. Dey, S. N. Tripathi, and M. Sharma (2006), Dust events in Kanpur, Northern India: Chemical evidence for source and implications to radiative forcing, *Geophys. Res. Lett.*, *33*, L08803, doi:10.1029/2005GL025278.

Chung, C. E., V. Ramanathan, D. Kim, and I. A. Podgorny (2005), Global anthropogenic aerosol direct forcing derived from satellite and ground-based observations, *J. Geophys. Res.*, *110*, D24207, doi:10.1029/2005JD006356.

Dey, S., and S. N. Tripathi (2007), Estimation of aerosol optical properties and radiative effects in the Ganga basin, northern India during the winter time, *J. Geophys. Res.*, *112*, D03203, doi:10.1029/2006JD007267.

Dey, S., S. N. Tripathi, R. P. Singh, and B. N. Holben (2004), Influence of dust storms on aerosol optical properties over the Indo-Gangetic basin, *J. Geophys. Res.*, *109*, D20211, doi:10.1029/2004JD004924.

Dey, S., S. N. Tripathi, R. P. Singh, and B. N. Holben (2005), Seasonal variability of aerosol parameters over Kanpur, an urban site in Indo-Gangetic basin, *Adv. Space Res.*, *36*, 778–782.

Dey, S., S. N. Tripathi, R. P. Singh, and B. N. Holben (2006), Retrieval of black carbon and specific absorption over Kanpur city, northern India during 2001–2003 using AERONET data, *Atmos. Environ.*, *40*, 445–456.

Doutriaux-Boucher, M., and G. Sèze (1998), Significant changes between the ISCCP C and D cloud climatologies, *Geophys. Res. Lett.*, *25*(22), 4193–4196.

Dubovik, O., and M. D. King (2000), A flexible inversion algorithm for retrieval of aerosol optical properties from Sun and sky radiance measurements, *J. Geophys. Res.*, *105*(D16), 20,673–20,696.

Dubovik, O., A. Smirnov, B. N. Holben, M. D. King, Y. J. Kaufman, T. F. Eck, and I. Slutsker (2000), Accuracy assessments of aerosol optical properties retrieved from Aerosol Robotic Network (AERONET) Sun and sky radiance measurements, *J. Geophys. Res.*, *105*, 9791–9806.

Ganguly, D., and A. Jayaraman (2006), Physical and optical properties of aerosols over an urban location in western India: Implications for shortwave radiative forcing, *J. Geophys. Res.*, *111*, D24207, doi:10.1029/2006JD007393.

Ganguly, D., H. Gadhavi, A. Jayaraman, T. A. Rajesh, and A. Misra (2005), Single scattering albedo of aerosols over central India: Implications for the regional aerosol radiative forcing, *Geophys. Res. Lett.*, *32*, L18803, doi:10.1029/2005GL023903.

Ganguly, D., A. Jayaraman, T. A. Rajesh, and H. Gadhavi (2006), Wintertime aerosol properties during foggy and non-foggy days over urban center Delhi and their implications for shortwave radiative forcing, *J. Geophys. Res.*, *111*, D15217, doi:10.1029/2005JD007029.

Girolamo, L. D., et al. (2004), Analysis of Multi-angle Imaging Spectro-Radiometer (MISR) aerosol optical depths over greater India during winter 2001–2004, *Geophys. Res. Lett.*, *31*, L23115, doi:10.1029/2004GL021273.

Hess, M., P. Koepke, and I. Schultz (1998), Optical properties of aerosols and clouds: The software package OPAC, *Bull. Am. Meteorol. Soc.*, *79*, 831–844.

Holben, B. N., et al. (1998), AERONET: A federated instrument network and data archive for aerosol characterization, *Remote Sens. Environ.*, *66*(1), 1–16.

Houghton, J. T., Y. Ding, D. J. Griggs, M. Nouguer, P. J. van der Linden, X. Dai, K. Maskell, and C. A. Johnson (Eds.) (2001). *Climate Change 2001: The Scientific Basis*, 881 pp., Cambridge Univ. Press, New York.

Jayaraman, A., H. Gadhavi, D. Ganguly, A. Misra, S. Ramachandran, and T. A. Rajesh (2006), Spatial variations in aerosol characteristics and regional radiative forcing over India: Measurements and modeling of 2004 road campaign experiment, *Atmos. Environ.*, *40*, 6504–6515.

Jethva, H., S. K. Satheesh, and J. Srinivasan (2005), Seasonal variability of aerosols over the Indo-Gangetic basin, *J. Geophys. Res.*, *110*, D21204, doi:10.1029/2005JD005938.

Kaufman, Y. J., O. Boucher, and D. Tanré (2002), A satellite view of aerosols in the climate system, *Nature*, *419*, 215–223.

Kaufman, Y. J., O. Boucher, D. Tanré, M. Chin, L. A. Remer, and T. Takemura (2005), Aerosol anthropogenic component estimated from satellite data, *Geophys. Res. Lett.*, *32*, L17804, doi:10.1029/2005GL023125.

King, M. D., S.-C. Tsay, S. E. Platnick, M. Wang, and K.-N. Liou (1998), Cloud retrieval algorithms for MODIS: Optical thickness, effective particle radius, and thermodynamic phase, *MODIS Algorithm Theor. Basis Doc. ATBD-MOD-05 MOD06–Cloud Product*, 57 pp., NASA Goddard Space Flight Cent., Greenbelt, Md.

King, M. D., W. P. Menzel, Y. J. Kaufman, D. Tanre, B.-C. Gao, S. Platnick, S. A. Ackerman, L. A. Remer, R. Pincus, and P. A. Hubanks (2003), Cloud and aerosol properties, precipitable water, and profiles of temperature and water vapor from MODIS, *IEEE Trans. Geosci. Remote Sens.*, *41*, 442–458.

Liou, K. N. (2002), *An Introduction to Atmospheric Radiation*, 583 pp., Elsevier, New York.

Massie, S. T., O. Torres, and S. J. Smith (2004), Total Ozone Mapping Spectrometer (TOMS) observations of increases in Asian aerosol in winter from 1979 to 2000, *J. Geophys. Res.*, *109*, D18211, doi:10.1029/2004JD004620.

Menon, S., J. Hansen, L. Nazarenko, and Y. Luo (2002), Climate effects of black carbon aerosols in China and India, *Science*, *297*, 2250–2253.

Moorthy, K. K., S. S. Babu, and S. K. Satheesh (2005), Aerosol characteristics and radiative impacts over the Arabian Sea during the intermonsoon season: Results from ARMEX Field Campaign, *J. Atmos. Sci.*, *62*, 192–206.

Pandithurai, G., R. T. Pinker, T. Takamura, and P. C. S. Devara (2004), Aerosol radiative forcing over a tropical urban site in India, *Geophys. Res. Lett.*, *31*, L12107, doi:10.1029/2004GL019702.

Pant, P., P. Hedge, U. C. Dumka, R. Sagar, S. K. Satheesh, K. K. Moorthy, A. Saha, and M. K. Srivastava (2006), Aerosol characteristics at a high altitude location in central Himalayas: Optical properties and radiative forcing, *J. Geophys. Res.*, *111*, D17206, doi:10.1029/2005JD006768.

Platnick, S., M. D. King, S. A. Ackerman, W. P. Menzel, B. A. Baum, J. C. Riédi, and R. A. Frey (2003), The MODIS cloud products: Algorithms and examples from Terra, *IEEE Trans. Geosc. Remote Sens.*, *41*(2), 459–473.

Podgorny, I. A., W. C. Conant, V. Ramanathan, and S. K. Satheesh (2000), Aerosol modulation of atmospheric and surface solar heating rates over the tropical Indian Ocean, *Tellus, Ser. B*, *52*, 947–958.

Ramachandran, S. (2005), Aerosol radiative forcing over Bay of Bengal and Chennai: Comparison with maritime, continental, and urban aerosol models, *J. Geophys. Res.*, *110*, D21206, doi:10.1029/2005JD005861.

Ramachandran, S., R. Rengarajan, A. Jayaraman, M. M. Sarin, and S. K. Das (2006), Aerosol radiative forcing during clear, hazy, and foggy conditions over a continental polluted location in north India, *J. Geophys. Res.*, *111*, D20214, doi:10.1029/2006JD007142.

Ramana, M. V., V. Ramanathan, I. A. Podgorny, B. B. Pradhan, and B. Shrestha (2004), The direct observations of large aerosol radiative forcing in the Himalayan region, *Geophys. Res. Lett.*, *31*, L05111, doi:10.1029/2003GL018824.

Ramanathan, V., and M. V. Ramana (2005), Persistent, widespread, and strongly absorbing haze over the Himalayan foothills and the Indo-Ganges basins, *Pure Appl. Geophys.*, *162*, 1609–1626.

Ramanathan, V., P. J. Crutzen, J. T. Kiehl, and D. Rosenfeld (2001a), Aerosols, climate and the hydrological cycle, *Science*, *294*, 2119–2124.

Ramanathan, V., et al. (2001b), Indian Ocean Experiment: An integrated analysis of the climate forcing and effects of the great Indo-Asian haze, *J. Geophys. Res.*, *106*, 28,371–28,398.

Ricchiazzi, P., S. Yang, C. Gautier, and D. Sowle (1998), SBDART: A research and teaching software tool for plane-parallel radiative transfer in the earth's atmosphere, *Bull. Am. Meteorol. Soc.*, *79*, 2101–2114.

Roderick, M. L., and G. D. Farquhar (2002), The cause of decreased pan evaporation over the past 50 years, *Science*, *298*, 1410–1411.

Satheesh, S. K. (2002), Radiative forcing by aerosols over Bay of Bengal region, *Geophys. Res. Lett.*, *29*(22), 2083, doi:10.1029/2002GL015334.

Satheesh, S. K., and V. Ramanathan (2000), Large differences in tropical aerosol forcing at the top of the atmosphere and Earth's surface, *Nature*, *405*, 60–63.

Satheesh, S. K., and J. Srinivasan (2006), A method to estimate aerosol radiative forcing from spectral optical depths, *J. Atmos. Sci.*, *63*(3), 1082–1092.

Satheesh, S. K., V. Ramanathan, X. Li-Jones, J. M. Lobert, I. A. Podgorny, J. M. Prospero, B. N. Holben, and N. G. Loeb (1999), A model for the natural and anthropogenic aerosols over the tropical Indian Ocean derived from Indian Ocean Experiment data, *J. Geophys. Res.*, *104*(D22), 27,421–27,440.

Satheesh, S. K., V. Ramanathan, B. N. Holben, K. K. Moorthy, N. G. Loeb, H. Maring, J. M. Prospero, and D. Savoie (2002), Chemical, microphysical, and radiative effects of Indian Ocean aerosols, *J. Geophys. Res.*, *107*(D23), 4725, doi:10.1029/2002JD002463.

Satheesh, S. K., J. Srinivasan, and K. K. Moorthy (2006), Spatial and temporal heterogeneity in aerosol properties and radiative forcing over Bay of Bengal: Sources and role of aerosol transport, *J. Geophys. Res.*, *111*, D08202, doi:10.1029/2005JD006374.

Singh, R. P., S. Dey, S. N. Tripathi, V. Tare, and B. N. Holben (2004), Variability of aerosol parameters over Kanpur, northern India, *J. Geophys. Res.*, *109*, D23206, doi:10.1029/2004JD004966.

Singh, S., S. Nath, R. Kohli, and R. Singh (2005), Aerosols over Delhi during pre-monsoon months: Characteristics and effects on surface radiation forcing, *Geophys. Res. Lett.*, *32*, L13808, doi:10.1029/2005GL023062.

Stamnes, K., S. Tsay, W. Wiscombe, and K. Jayaweera (1988), Numerically stable algorithm for discrete-ordinate-method radiative transfer in multiple scattering and emitting layered media, *Appl. Opt.*, *27*, 2502–2509.

Strahler, A. H., et al. (1999). MODIS BRDF/Albedo Product: Algorithm Theoretical Basis Document Version 5.0, NASA Goddard Space Flight Cent., Greenbelt, Md. (Available at http://modis.gsfc.nasa.gov/data/atbd/land_atbd.php)

Tare, V., et al. (2006), Measurements of atmospheric parameters during Indian Space Research Organization Geosphere Biosphere Program Land Campaign II at a typical location in the Ganga Basin: 2. Chemical properties, *J. Geophys. Res.*, *111*, D23210, doi:10.1029/2006JD007279.

Taylor, J. R. (1982), *An Introduction to Error Analysis: The Study of Uncertainties in Physical Measurements*, pp. 3–91, Univ. Sci. Books, Sausalito, Calif.

Tripathi, S. N., S. Dey, V. Tare, and S. K. Satheesh (2005a), Aerosol black carbon radiative forcing at an industrial city in northern India, *Geophys. Res. Lett.*, *32*, L08802, doi:10.1029/2005GL022515.

Tripathi, S. N., S. Dey, V. Tare, S. K. Satheesh, S. Lal, and S. Venkataramani (2005b), Enhanced layer of black carbon in a north Indian industrial city, *Geophys. Res. Lett.*, *32*, L12802, doi:10.1029/2005GL022564.

Tripathi, S. N., S. Dey, A. Chandel, S. Srivastava, R. P. Singh, and B. N. Holben (2005c), Comparison of MODIS and AERONET derived aerosol optical depth over the Ganga basin, India, *Ann. Geophys.*, *23*, 1093–1101.

Tripathi, S. N., et al. (2006), Measurements of atmospheric parameters during Indian Space Research Organization Geosphere Biosphere Programme Land Campaign II at a typical location in the Ganga basin: 1. Physical and optical properties, *J. Geophys. Res.*, *111*, D23209, doi:10.1029/2006JD007278.

Tripathi, S. N., A. Pattnaik, and S. Dey (2007a), Aerosol indirect effect over the Indo-Gangetic Basin, *Atmos. Environ.*, *41*(33), 7037–7047.

Tripathi, S. N., A. K. Srivastava, S. Dey, S. K. Satheesh, and K. K. Moorthy (2007b), Atmospheric heating rate altitude profiles due to black carbon aerosols at Kanpur (northern India), *Atmos. Environ.*, *41*(32), 6909–6915.

Yu, H., et al. (2006), A review of measurement-based assessments of the aerosol direct radiative effect and forcing, *Atmos. Chem. Phys.*, *6*, 613–666.

S. Dey and S. N. Tripathi, Department of Civil Engineering, Indian Institute of Technology, Kanpur 208016, India. (snt@iitk.ac.in)